Koninklijk Nederlands
Meteorologisch Instituut
Ministerie van Infrastructuur en Milieu

Cold winters and the relation to atmospheric blocking

Hylke de Vries

De Bilt, 2011 | Technical report; TR-324

Koninklijk Nederlands
Meteorologisch Instituut
Ministerie van Infrastructuur en Milieu

Cold winters and the relation to atmospheric blocking

Versie 1.0

Datum 12 september 2011
Status Definitief

COLD WINTERS AND THE RELATION TO ATMOSPHERIC BLOCKING

HYLKE DE VRIES

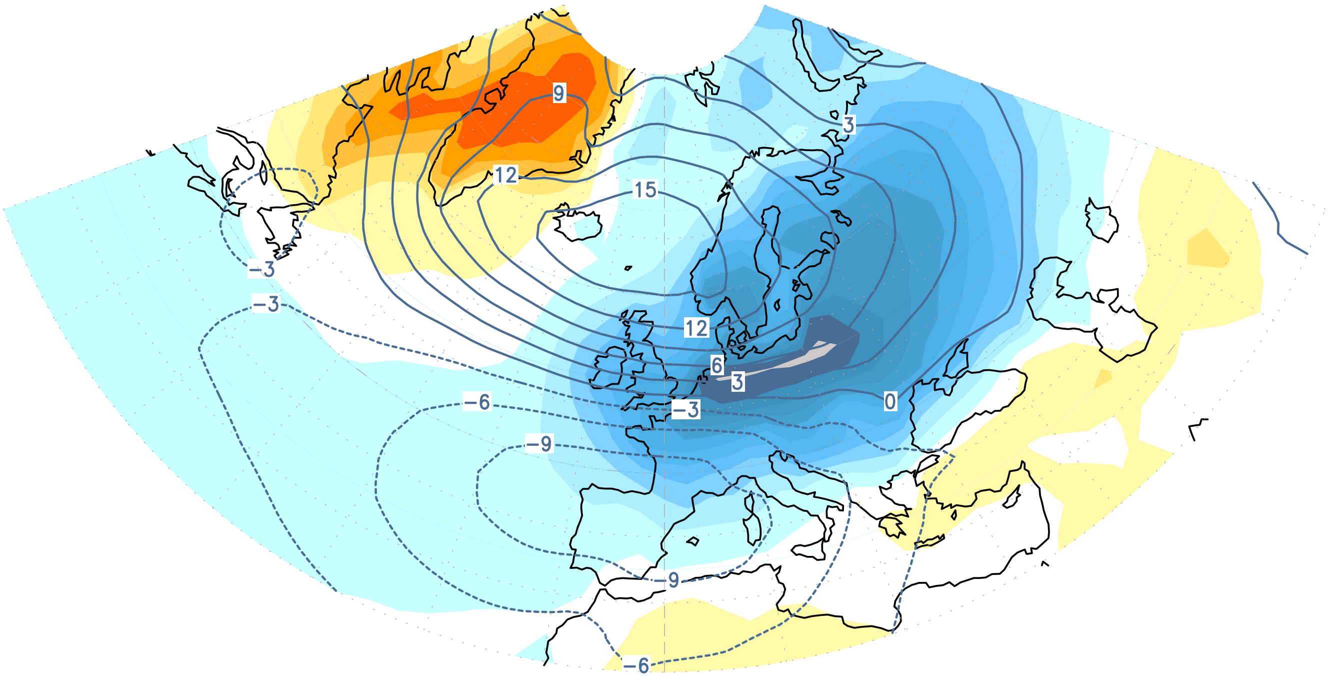

JANUARY 3, 2011

ROYAL NETHERLANDS METEOROLOGICAL INSTITUTE
POBOX 201, 3730 AE, DE BILT, THE NETHERLANDS

COLD WINTERS AND THE RELATION TO ATMOSPHERIC BLOCKING

A report to GasTerra and NAM describing research undertaken at KNMI between September 2009 and September 2010. Project-title: "Blokkades and Klimaatverandering" (Atmospheric Blocking and Climate Change).

Cover: Anomaly composite fields of mean sea-level pressure (contours) and 2-meter temperature (colors, ranging from -10 to +10 degrees Celcius), obtained for the 1% coldest days in the Netherlands (measured with effective temperature). Data source: ERA-40 reanalysis data (Uppala et al., 2005). For more details see Figure 4.2 on page 33 of this report.

EXECUTIVE SUMMARY

This report discusses the relation between cold temperatures over the Netherlands and large-scale anomalous circulation and temperature patterns over Europe and the North Atlantic. The report has been split in two parts: 'Cold Winters' and 'Cold Spells'. Part I, 'Cold Winters' addresses the local and large-scale structure of heating degree days of entire winters, thereby focussing on the climatological aspects (Chapter 3). Part II, 'Cold Spells', describes more the 'weather'-related aspects of shorter cold periods (Chapters 4-6).

Chapter 3 demonstrates the geographical extent of cold European winters and shows that winters that are anomalously cold in the Netherlands are also cold in a large part of Europe. Chapters 4 and 5 investigate the large-scale pressure patterns that go along with cold spells. Two different patterns are found, characterized by anomalously high pressures over the Greenland Iceland region, and the Scandinavia Russia region. Particularly the latter pattern is associated with very high pressures and a large horizontal extent. Both patterns have in common that the prevailing westerly winds are blocked. Chapter 6 discusses the subject of persistence of cold spells. It is more likely to stay cold if it is already cold for some days. The optimum probability is found for events that last already between 10 and 20 days. Under the A1B emission scenario and using climate model output (ESSENCE data), there is a significant drop in the probability for a cold-spell event to last longer for the period 2051-2100.

Since persistent cold spells are associated with atmospheric blocking this observation calls for further investigation of in particular the persistence of atmospheric blocking under future climate scenarios. Note that the statements about the future climate state were inferred from climate model output from a one particular model (ESSENCE) and one particular emission scenario (A1B). Other data sets obtained with different climate models should be examined in order to investigate uncertainties related to model error.

The following few pages give a more detailed summary of the main undertakings (in bold) and conclusions (in bullets) of the two parts ('Cold Winters' and 'Cold Spells') of the report.

PART I: COLD WINTERS

Heating degree days (chapter 3)

Heating degree days $D(\bar{T})$ equals the sum of all daily-mean temperatures $\bar{T}$ below 18.0 degrees in the winter half year (October-March). Therefore, $D(\bar{T})$ provides an integral measure of the winter heat budget.

Present-day climate

- *Structure*: The climatology of $D(\bar{T})$ over Europe shows large positive South-North and West-East gradients (Fig. 3.3). The lowest values of D are found near the coastal areas and at open sea, the largest values over Scandinavia, Siberia and mountainous areas.
- *Anomalies*: Cold (or mild) winters over the Netherlands are also cold (or mild) in large parts of Western and Central Europe (Fig. 3.4), thereby suggesting a large-scale common origin.
- *Wind*: Low temperatures in combination with strong winds increase gas demand. Taking this into account by computing $D(T_{eff})$, ($T_{eff} = \bar{T} - 2/3\bar{U}$, with $\bar{U}$ the wind speed), coastal and open-sea areas show the largest increase (Fig. 3.3).

Future projections

- *Decrease of D*: Simulations with a climate model and the A1B emission scenario shows a sharp drop in $D(\bar{T})$: between 20 and 30% for large parts of Europe near the end of the 21st century (Fig. 3.9). For the Netherlands this corresponds to an average winter temperature increase of about 2.5 degrees.
- *Changes accelerate*: According to ESSENCE (Fig. 3.6), the decrease will be faster in the 2051-2100 period (-58 per decade) than it has been in the 1951-2000 period (-28 per decade).
- *Comparison*: Comparing current to possible future climate conditions, one can conclude that winters which are exceptionally mild given current climate conditions will become ordinary "average" winters near the end of the 21st century.
- *Disclaimer*: The future climate state was obtained using only a single climate model and one particular emission scenario. Other data sets obtained with different climate models should be examined in order to investigate uncertainties related to model error.

Recommendations (chapter 3)

- *Focus on large scales*: Climate models have difficulties in producing local climate at continental boundaries (e.g., Netherlands), but are expected to give more reliable results over larger domains. Keep focusing on the large scales that are typically well resolved.
- *Multi-model output*: Assess uncertainty due to model error by incorporating output from other climate models.

PART II: COLD SPELLS

Composite analysis (chapter 4)

A composite analysis yields information about the mean atmospheric state that satisfies particular threshold criteria. The focus is on the 1% and 5% coldest (measured in $\bar{T}$ and T_{eff}) days over the Netherlands.

Present-day climate

- *Climatological Westerlies*: The European winter pressure climatology involves a large-scale low pressure system with its center near Greenland and Iceland, and high pressures near the Azores. This dipole produces the typical South-Westerly wind patterns in our region (Fig. 4.1). The atmosphere is said to be in a blocked state, if the climatologically predominant Westerlies are absent or have reversed sign.

• *Blocking-high*: The composite of mean sea-level pressure for the 1% coldest T_{eff} has high pressure over Scandinavia and Greenland, resulting in South-Easterly winds over the Netherlands (Fig. 4.1). This confirms the hypothesis that extreme cold days most often occur during atmospheric blocking. This pattern is robust to changes in the geographical location where the threshold criterion is applied (Fig. 4.5).

• *Bias to second half of winter*: The distribution of the 1% coldest days has a clear bias towards the second half of the winter half year (Table 4.1), caused primarily by the proximity of the North Sea.

• *Persistent pattern*: The blocking high-pressure pattern exists for at least two weeks at a similar geographical location (center between Iceland and Scandinavia). During this period cold air originating in Siberia is transported (Fig. 4.3). On the western flank of the high pressure pattern, Greenland experiences anomalous heating.

Future projections

• *Bias to second half of winter*: ESSENCE predicts no major change in 'timing' of the coldest day events. Note that ESSENCE itself has a stronger bias towards the second half of the winter than the reanalysis data.

• *Disclaimer*: The future climate state was obtained using only a single climate model and one particular emission scenario. Other data sets obtained with different climate models should be examined in order to investigate uncertainties related to model error.

Recommendations (chapter 4)

• *Composites for future projections*: Carry out further composite analysis for the future projections, in particular the issue of the persistence of blocking high pressure and the possible changes thereof in future.

• *Multi-model output*: Assess uncertainty due to model error by incorporating output from other climate models.

Cluster analysis (chapter 5)

Physically distinct patterns can satisfy similar threshold conditions. Cluster analysis is used to further examine the mean sea-level pressure (mslp) composite associated with anomalously cold days in De Bilt.

Present-day climate

• *Two clusters*: Cluster analysis of the mslp fields associated with the 1% coldest days reveals two distinct patterns (Fig. 5.2). The first pattern (G) has its high pressure over Greenland and forms a tripolar structure with accompanying lows to the south-west and north-east of the high. The second pattern (S) has a much larger horizontal scale with the center high pressure region located over Scandinavia and Russia, and low pressures over Greenland.

• *Blocked flow*: Both clusters G and S are related to conditions where the prevailing climatological westerly winds over the Netherlands and a large part of central Europe are blocked. Moreover, each of these is immediately recognised as being relevant to winter-time cold spells by a skilled meteorologist.

Future projections

• *Two clusters*: The two dominant cluster structures for the future coldest days are very similar to those obtained for present-day climate, although the temperature threshold is several degrees higher (Fig. 5.5). Also the timing of the events is not predicted to change significantly (Table 5.2).

• *Disclaimer*: The future climate state was obtained using only a single climate model and one particular emission scenario. Other data sets obtained with different climate models should be examined in order to investigate uncertainties related to model error.

Recommendations (chapter 5)

• *None particularly.*

Persistence (chapter 6)

Often a cold day is followed by another. Changes in the persistence of cold weather are important for the gas industry. This subject is investigate by computing the probability for getting another cold day if it is already cold for some days.

Present-day climate

- *Probabilities*: The probability p for a cold spell (defined here as belonging to the 5% coldest days) to last another day increases with the duration of the event (Fig. 6.1-6.2). The optimum ($p \sim 0.8$) is found for events that last already between 10 and 20 days. The probability that it will stay cold for n more days, given that it is already cold for some days, quickly decreases with increasing n. At any point during a cold-spell it is found that the probability that it will stay cold for at least another 5 days never exceeds $p = 0.5$.
- *Return periods* were estimated for cold spells of a given duration (Fig. 6.3). It is found that the return period for cold spells of ten days is about 5 years, and that of a cold spell of twenty days about twenty years.

Future projections

- *Probabilities drop*: Under the A1B scenario and using climate model output (ESSENCE data), there is a strong drop in the probability for a cold-spell event to last another day for the period 2051-2100 (Fig.6.4), if the same threshold is chosen as used for the reference period (1958-2002 obtained using ERA40 data).
- *Different threshold*: Some of the drop in probability is accounted for by using the 2051-2100 period's own 5% temperature threshold (which is almost 4 degrees higher). If that threshold is used for the future scenario, it is still observed that the probability for getting a prolonged cold period becomes smaller (Fig. 6.5). For events that last only a few days, the changes in p are not observed.
- *Disclaimer*: The future climate state was obtained using only a single climate model and one particular emission scenario. Other data sets obtained with different climate models should be examined in order to investigate uncertainties related to model error.

Recommendations (chapter 6)

- *Persistence versus blocking* Since the long cold spells are mostly associated with atmospheric blocking, this calls for a further investigation of persistence of blocking in future. The recommendation is to investigate the relation between changes in persistence of cold-spells and changes in persistence of atmospheric blocking in more detail.
- *Multi-model output*: Assess uncertainty due to model error by incorporating output from other climate models.

Contents

Introduction and Preliminaries

1 | Introduction

This report describes the research carried out under the GasTerra/NAM project.

1 Weather and Climate

Living in a country where the weather is extremely variable, people in the Netherlands (almost) invariably like discussing the weather. When the winter season (October to March) approaches, typical questions are discussed. When will the first snow fall? Will we get a period with temperatures low enough to make ice-skating on the lakes and canals possible? Will we get another 'Elfstedentocht' ("It should be, shouldn't? We've had none for so long")? Such questions are not easy, if not impossible to answer exactly. What are the reasons behind this? What prevents us from predicting with high chance of success the occurrence of a cold winter, or more generally, the weather on time scales longer than roughly ten days? The short answer is that observations suggest that the atmosphere is highly chaotic. The consequence of chaoticity is the often quoted 'butterfly-effect', first termed so by Lorenz (1963). The butterfly-effect describes the possible effect of a flying butterfly (small spatial scale) somewhere in the Brasilian rainforest, on the development of a major storm (large scale) a few days later over Western Europe. In this description, the butterfly is used as a metaphor for extreme sensitivity to initial conditions. Apparently, our earth-ocean-atmosphere system is in such a state that even the slightest initial disturbance (such as an observational error) will quickly accumulate and influence the larger (observed) scales. The limited observational network inevitably confronts us with a predictability horizon. Beyond this horizon deterministic forecasts made with a single model quickly loose their validity.

It is important to note that chaotic should not be read as 'completely random'. For suppose we knew all equations describing the evolution of all variables (like for example temperature, pressure and wind, ocean state etc) exactly, then, in theory at least, one could predict the future state of the system by solving these equations with an accurate numerical algorithm (even if the system were chaotic). With a random process this would not be possible. However, the solvability of the future state requires an exact description of the current state of the system and exact knowledge of the equations governing their evolution. Unfortunately, we have neither. First (and possibly foremost) we do not know the current state of the earth-atmosphere system exactly (e.g., the clapping wings of the butterfly in the distant Brasilian rainforest). There are uncertainties in the observations. These uncertainties result in initial-condition errors. Second, we do not know all equations. In fact, many aspects of the earth-atmosphere evolution are 'parameterized', which means that we describe the behaviour using approximate equations that involve one or more empirically determined parameters. The errors introduced by the imperfections of the model will be termed model-error.

Researchers nowadays use statistical techniques to assess or even to improve the reliability of forecasts. All major weather prediction centers use ensemble techniques where a whole ensemble of forecasts is created (often at lower resolution to reduce computational costs), that start from slightly perturbed initial conditions. In many cases it is found that the ensemble-mean better describes the future state than the future state described by the single model run. Moreover, by using the ensemble, one also gets approximate knowledge of the probability density function, which describes the chance of occurrence. Unfortunately it is rather less trivial to overcome the problems associated with model error and much research is being undertaken to tackle this problem (e.g., multi-model ensembles, ensembles with perturbed physics).

2 Climate Scenarios (KNMI '06)

In recent years, KNMI has created scenarios (referred to as KNMI '06 scenarios) for the future climate of the Netherlands (Hurk et al., 2006; Klein Tank and Lenderink, 2009). The next scenarios are expected to be published in 2013. Climate scenar-

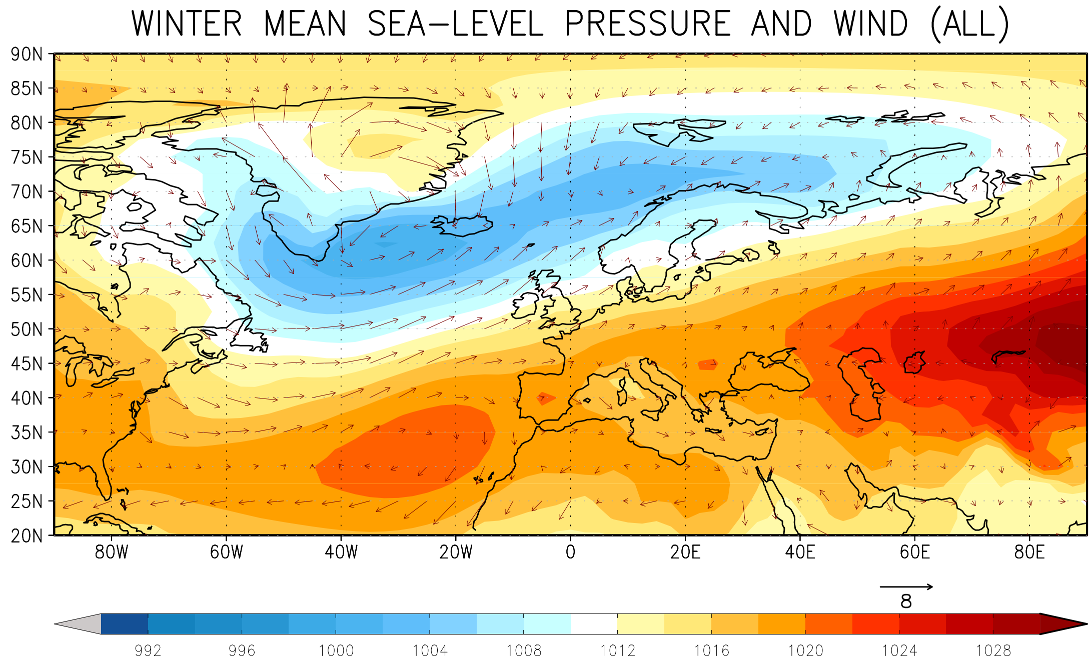

Figure 1.1: Mean sea-level pressure and 10M wind for the winter (October to March) climatology of ERA40.

ios are consistent and plausible projections of the climate in to the future. They have been realized using a combination of observations, and output from regional and global climate models. Parameters that influence climate in the Netherlands the most, are temperature and circulation. Changes in just these two parameters only, lead to a two-dimensional space of all future climatic states in the Netherlands. The KNMI '06 scenarios consider changes in these two parameters, and their subsequent impact on other parameters like precipitation and wind. For temperature they consist of a mild (+1 degree) or stronger (+2 degree) temperature increase (in 2050 compared to 1990). For circulation they consist of no-change or change. The scenarios that are formed from the four possible combinations approximately describe the four corners of a square of most likely future climatic states within the Netherlands. A further assumption in the scenarios is that regional (i.e., within the Netherlands) climatic differences in future will be comparable to those differences in current climate.

When global climate models are run forward in time to obtain information over the future climate, they depend on estimations of (rates of) greenhous gas emissions and aerosols. These estimates in turn depend on hypotheses about the future development of world population, economy and technological development. In the 2007 report of the Intergovernmental Panel on Climate Change (IPCC), different emission-scenarios are investigated. These lead to a predicted increase of global mean temperature in 2100 between 1 and 6 degrees Celcius by 2100. In order to sample the uncertainty as accurately as possible, many different climate models have been run assuming the same emission scenario. Up to 2050 the inter-model differences (with regard to e.g. global mean temperature) mostly exceed the predicted change resulting from the differences in the emission-scenarios. This emphasizes that the largest part of the uncertainty in 2050 still results from our limited understanding of the climate system. The KNMI '06 scenarios can not be mapped one to one to these IPCC emission-scenarios (Klein Tank and Lenderink, 2009) since the former were not based on the emission-scenarios, but on the changes in the global mean temperature. Therefore the global mean temperature provides an indirect link. For the period up to 2050, each of the four KNMI '06 scenarios can occur for each of the emission scenarios (Klein Tank and Lenderink, 2009).

It is important to realize that an increase of global mean surface temperature of say one degree Celcius, does not imply that the temperature is increased uni-

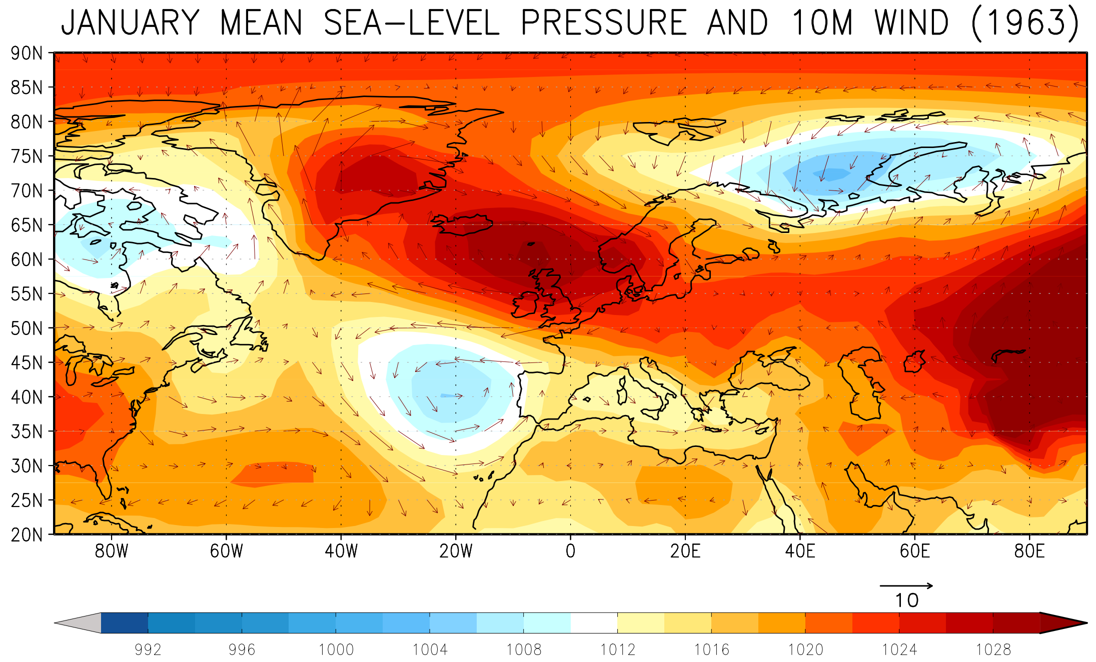

Figure 1.2: Mean sea-level pressure and 10M wind for January 1963.

formly and everywhere with one degree. There will be large geographical differences. Seas, for instance, will heat only very slowly, while the continents heat much faster. Poles are expected to heat faster than other regions. The geographical changes in the heat distribution will further impact on the circulation, which may in turn lead to changes in local processes. Following the KNMI '06 scenarios the winters in the Netherlands will get milder and wetter, although no major changes in the wind-climate (i.e. number of storms per winter) are expected. The central aim of this report is to investigate the conditions that are associated with cold weather over the Netherlands and Western Europe.

3 Atmospheric Blocking and Cold Winters

At midlatitudes, the climatologically prevailing winds come from the West (called *Westerlies*). These Westerlies are a direct consequence of the fundamental balances that exist in the atmosphere-ocean system. Figure 1.1 (page 12) shows the winter-mean wind speed at 10M altitude and the mean sea-level pressure distributions for the Euro-Atlantic region. As one can see there is a large-scale pressure pattern with low pressures in the North and high pressures near the Azores. The resulting winds are a consequence of on the one hand the tendency of the air to flow from high to low pressures and on the other hand the rotation of the Earth. They are responsible for transporting the moist, relatively mild air towards Western Europe.

As said above, the Westerlies are caused by fundamental physical balances. However, this existing balance does not prohibit the formation of large-scale anomalies. To the contrary, large-scale 'anomalies' of this Westerly circulation are of vital importance to the atmosphere, as they (together with the Ocean currents) play a crucial role in maintaining the net poleward heat transport. They are constantly being created and destroyed by a process called baroclinic instability. Without such anomalies, the equator would get warmer and warmer, whereas the poles would get colder and colder.

When analyzed in terms of the mean sea-level pressure field, the anomalies take the form of so-called cyclones or storms (large-scale low-pressure systems), and anti-cyclones (high-pressure systems). The wind fields associated with such cyclones and anti-cyclones follow simple rules: counter-clockwise around a low-pressure system, and clockwise around a high-pressure

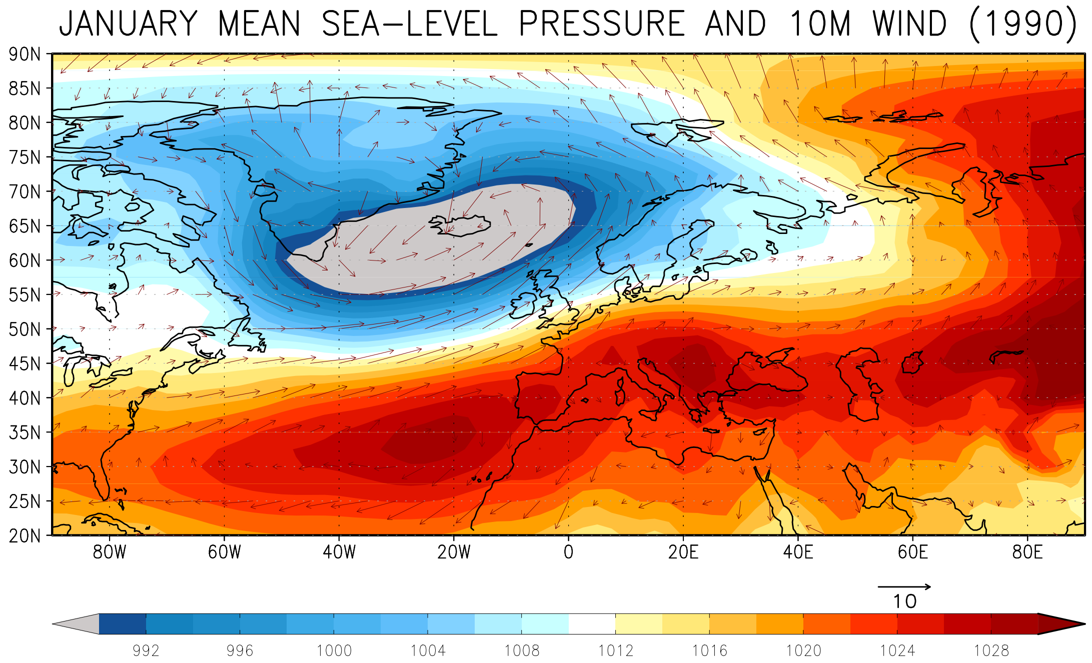

Figure 1.3: Mean sea-level pressure and 10M wind for January 1990.

system. It immediately follows from these rules that a high-pressure system to the North of the Netherlands will result in reduced, or even reversed Westerlies. In this sense, the high-pressure anti-cyclone leads to a 'blocking' of the climatologically prevailing Westerlies.

There is a simple direct link between anomalous circulation patterns and anomalous temperature distributions. Due to the lack of sunshine, the Northern Hemisphere (NH) cools significantly during the winter season. Since seas and oceans have a large heat capacity or 'memory' (they store a lot of heat inside their volume), it takes a long time to cool them. The land, on the other hand, has much shorter 'memory' and cools more rapidly. Therefore persistent easterlies will lead to colder than usual conditions in winter and warmer than usual conditions in summer. The large heat capacity of the sea also explains why in coastal regions of Western Europe the second half of the climatological winter is markedly colder than the first half.

Two striking examples of these altered flow conditions are shown in Figure 1.2 (page 13) and 1.3 (page 14). These figures show the average mean sea-level pressure and 10m winds for January 1963 and 1990 respectively. Focussing on the January 1963 case, there are high pressures in the North and low pressures in the South, with the Azores high being pushed further even further South. Contrast this flow state to the climatology shown in Figure 1.1. The differences could hardly be larger. The high-pressure 'block' led to easterly winds throughout January and very low temperatures. The example in Figure 1.3 shows the exceptionally mild January of 1990. In this case, the Westerlies are stronger than usual in our region, because the North-South pressure differences are much stronger than those obtained for the climatology.

Although the above rationale is intuitively clear, on shorter time-scales reality is more complicated. Indeed, a high-pressure system over Northern Europe will set up a transport of air that originates in (cold) Siberia and hence will lead to colder than usual (climatological) conditions over Netherlands and Western Europe. Similarly, a large-scale cyclone (low-pressure system) at a similar location will lead to milder than usual conditions due to the transport of air that originated over the warm Atlantic. However, whether or not such a blocking anti-cyclone or cyclone (i.e., the anomaly) will lead to conditions that are significantly colder or warmer respectively, depends on more details of the meteorological conditions. Particularly important are the temperature patterns, that existed prior to the formation of the anomaly, and the duration or persistence (and near stationarity) of the anomalous flow conditions. Many of these aspects are directly or indirectly relevant to the gas industry and will be addressed in this report.

4 What lies ahead

In this report an account is given of the local and large-scale meteorological conditions that accompany cold weather over the Netherlands and Western Europe. Two different time scales are discussed: (1) entire winters and (2) cold weather periods (called *cold spells* from here). In our opinion such a separation of time scales is useful, since the former provides (and requires) knowledge about the current (and future) climate, whereas the latter provides (and requires) knowledge about the weather. For each part we have made a further division into present-day climate (1960-2000) and future projections (2050-2100). For the future projections, climate model data has been used for one particular emission-scenario, which in the IPCC report is referred to as the A1B scenario. In terms of the increase of global mean temperature, the A1B emission scenario produces changes between 1.5 and 4 degrees. Note that we have used output from only one single climate model. When reading sections on the future-perspective one should therefore keep in mind that apart from the uncertainty in the realism of the emission-scenario, there is also a significant part of the uncertainty that has not been taken in to account by focusing on a single model.

The next chapter introduces two commonly used variables, *heating degree days* and *effective temperature*, as well a description of the data sources that have been used. Thereafter we continue with the part of the report on ‘Cold Winters’, followed by the part on ‘Cold Spells’. In ‘Cold Winters’ the local and large-scale structure of heating degree days is analysed, based on observational data, as well as climate model data. The latter has been obtained for current climate conditions as well as for future projections. In ‘Cold Spells’ several (statistical) techniques, such as composite analysis and clustering analysis have been used to get more insight in to the meteorological conditions involved with cold spells. A final chapter on the ‘persistence’ of cold spells is added.

2 Variables and Data

This chapter describes commonly used variables as well as the data sources used in the study.

1 Variables

1.1 *Effective temperature*

Various factors determine gas demand. Most obviously, gas demand is influenced by temperature. Furthermore, 'wind chill' not only influences human beings, it also affects buildings. The effect of wind speed can be measured and is generally in the direction of larger gas demand. Other factors, such as cloudiness and humidity also play a role but their effect is not taken into account in this study. Following Wever (2008), effective temperature is defined as

$$T_{eff} = \bar{T} - \frac{2}{3}|\bar{U}|, \tag{1.1}$$

where $\bar{T}$ is the daily mean temperature [^{o}C] and $|\bar{U}|$ is the daily mean wind speed [m s^{-1}]. The factor 2/3 has been determined empirically.

1.2 *Heating degree days*

One of the many possible ways to assess the 'strength' of an entire winter half year (or any other time interval), is by computing the so-called heating degree days D, which is defined as

$$D(\bar{T}) = \sum_{all\ days} \max(T_{threshold} - \bar{T}, 0), \tag{1.2}$$

where D has units ^{o}C day. In (1.2) above, the assumption is that gas is being used (for heating) whenever the daily mean temperature falls below $T_{threshold} \equiv 18\ ^o$C. For this threshold, the timeseries of yearly D values correlates well with total winter gas demand. However, as already noted by Wever (2008), for all winter days at De Bilt in the period from 1904 upto 2007 there were only 4 days where the threshold of 18^{o}C was exceeded, implying that (at least for De Bilt) there is a strong relation between gas demand and the mean winter temperature.

2 Data

2.1 *Present day*

The results of the following chapters have been obtained mostly using data from the ERA-40 reanalysis project (Uppala et al., 2005). This data set, which describes the state of the atmosphere between September 1957 and August 2002, has been produced with a recent version of the ECMWF model using a process called data assimilation. With data assimilation all available observations (e.g., in situ measurements, radiosondes, aircrafts, ships, satellites) are combined to produce the best available estimate of the true global atmospheric state (called analysis) at 6-hourly intervals. The 'observations density' is generally very high over densely populated areas such as Western and Central Europe. Therefore we may expect a reliable reanalysis product over these regions. However, observations are relatively scarce over large parts of the oceans and over Antarctica which may result in possibly large (but unknown) deviations from the true state of the atmosphere.

2.2 *Future projections*

For the projections in to the future, we use climate-model output from the ESSENCE project (Sterl et al., 2008). In ESSENCE a 17-member ensemble was created to simulate future climate following the A1B emission scenario. Each ensemble member consists of a single 150-year run (1950-2100). Apart from these 17 ensemble members there are twenty simulations of the 1950-2000 period, which serve as a control run. The output from these control simulations is used to compare the ESSENCE data to the ERA-40 data for current climate conditions.

There are small differences between the climatology of $D(\bar{T})$ of ESSENCE and ERA-40 for the control period. In terms of surface temperature, Northern Scandinavia is a bit too cold compared to ERA-40. The variability is very similar for the two dataset. For this reason we have not further calibrated the ESSENCE data set to European climate, except in certain cases. These exceptions will be mentioned explicitly.

I

Cold Winters

3 Heating degree days

Abstract. This chapter discusses the heating degree days from local to regional scale.

Conclusions. • Heating degree days $D(\bar{T})$ computed for the winter half year show large positive South-North and West-East gradients (Fig. 3.3). The lowest values of $D(\bar{T})$ are found near the coastal areas and at open sea and the largest values over Scandinavia, Siberia and mountainous areas. • If the effect of the wind is taken into account, by computing $D(T_{eff})$, the coastal and open sea areas show the largest increase in heating degree days (Fig. 3.3). • Anomalously cold (or mild) winters over the Netherlands are also cold (or mild) in large parts of Western and Central Europe, hinting on a common large-scale origin that produces the anomalous winter conditions (Fig. 3.4). • Under the A1B emission scenario daily mean winter temperatures will rise several degrees by the end of the 21st century. This increase of temperature impacts on $D(\bar{T})$ which is expected to decrease 20 and 30% for large parts of Europe (Fig. 3.9). For the Netherlands this corresponds to an average winter temperature increase of about 2.5 degrees. • According to ESSENCE (Fig. 3.6), the decrease will be faster in the 2051-2100 period (-58 per decade) than it has been in the 1951-2000 period (-28 per decade). • Comparing current to possible future climate conditions for the Netherlands, one can conclude that winters which are among the mildest given current climate conditions, are projected to become "average" winters near the end of the 21st century.

1 Introduction

Heating degree days D, as defined in (1.2), is a commonly used variable for measuring the total 'intensity' of a winter, where anomalously high (low) values of D correspond to cold (mild) winters. In this chapter D is analyzed for current climate conditions, as well as for future climate projections. Two definitions of D are used, one which is based on the daily mean temperature, $D(\bar{T})$, and one which is based on daily-mean *effective* temperature, $D(T_{eff})$. The Netherlands are located at the transition zone between major sea areas (Atlantic Ocean) and land areas (Eurasian continent). These transition zones are notoriously difficult to simulate using climate models. Therefore, when using climate-model output, as will be done for the future projections, it is important to understand how anomalously high and low values of D locally (over the Netherlands) relate to large-scale anomalous conditions. This large-scale perspective of heating degree days is topic of this chapter.

2 Present day

2.1 *Local scale*

Figure 3.1 shows total winter $D(\bar{T})$ as a function of the years. Clearly, there are large year-to-year fluctuations. The least-square fit suggests that there is a downward trend with time. Famous winters like 1963 (and in fact most "11-stedentocht winters") clearly stand out. The year 1990 was a year with very low $D(\bar{T})$. For this year, and for the coldest in the series (1963), we will study the large-scale perspective as well. Also shown in Figure 3.1 is the year-to-year autocorrelation function of $D(\bar{T})$, along with a 95% confidence interval. This figure shows that one cannot tell from the data whether a cold year will be followed by another (see also Wever (2008) who used this technique for the yearly minimum values of T_{eff}.)

Figure 3.2 shows a frequency distribution or histogram of $D(\bar{T})$ (left) and $D(T_{eff})$ (right). There is a strong impact of the wind over the Netherlands, which leads to significantly higher values. The shape of the two distributions is also different. This difference can be explained partly from the fact that strong winds often go along with relatively mild temperatures, thereby giving a substantial contribution to $D(T_{eff})$ but not to $D(\bar{T})$.

2.2 *Regional to Global Scale*

Figure 3.3 shows the mean climatology of heating degree days $D(\bar{T})$ computed using ERA-40 reanalysis data. There are large North to South and East to West differences in $D(\bar{T})$, with Siberia and the mountainous areas (Scandinavia, Alps, Turkish highland) clearly standing out. Due to the absence of significant topogra-

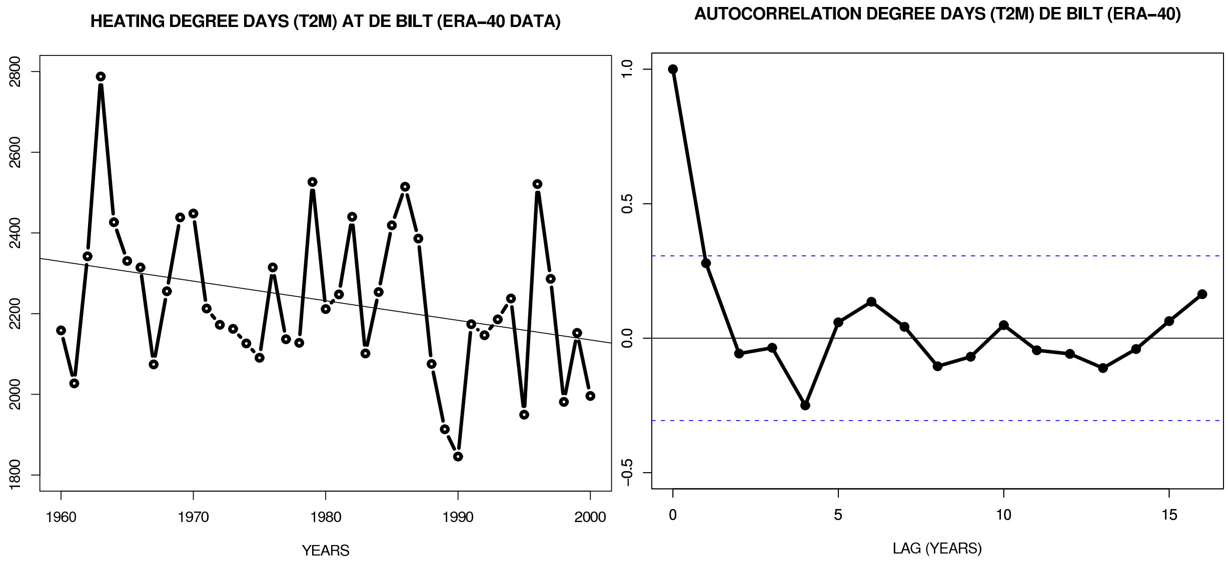
HEATING DEGREE DAYS (T2M) AT DE BILT (ERA–40 DATA)

AUTOCORRELATION DEGREE DAYS (T2M) DE BILT (ERA–40)

Figure 3.1: (left) Total winter values of heating degree days $D(\bar{T})$ as a function in time for the ERA-40 period (1960-2000). The threshold $T_{threshold}$ = 18.0 was used to determine $D(\bar{T})$ [see (1.2)]. The drawn line is the least-square fit through the data. (right) Year-to-year autocorrelation function with 95% confidence interval, which was obtained using bootstrap methods.

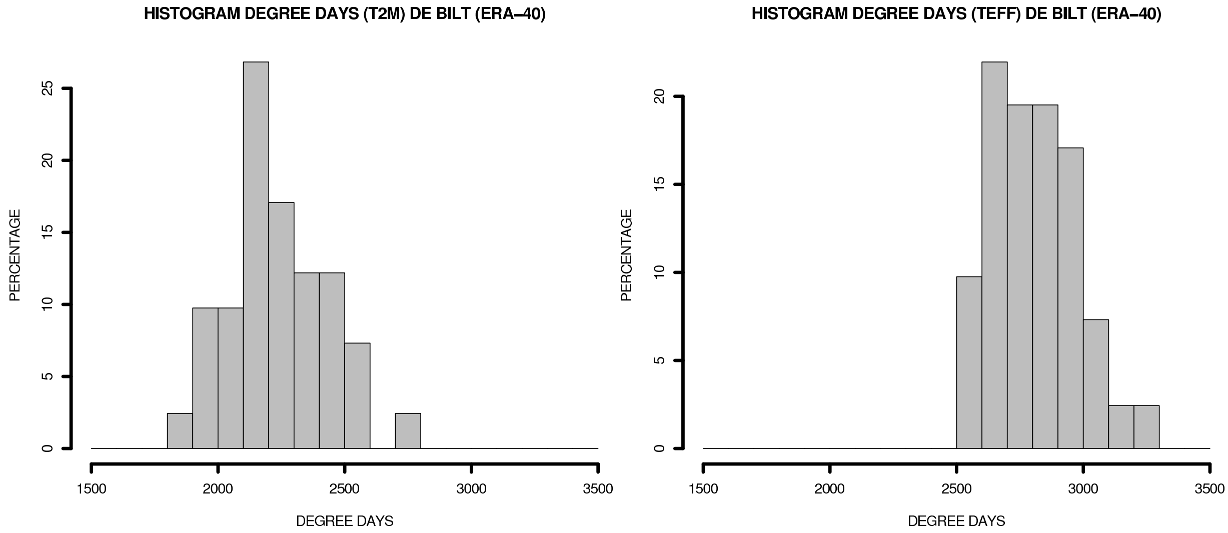
HISTOGRAM DEGREE DAYS (T2M) DE BILT (ERA–40)

HISTOGRAM DEGREE DAYS (TEFF) DE BILT (ERA–40)

Figure 3.2: Histogram of total winter values of (left) D for the ERA-40 period (1960-2000). The threshold $T_{threshold}$ = 18.0 was used to determine D [see (1.2)]. (left) $D(\bar{T})$; (right) $D(T_{eff})$.

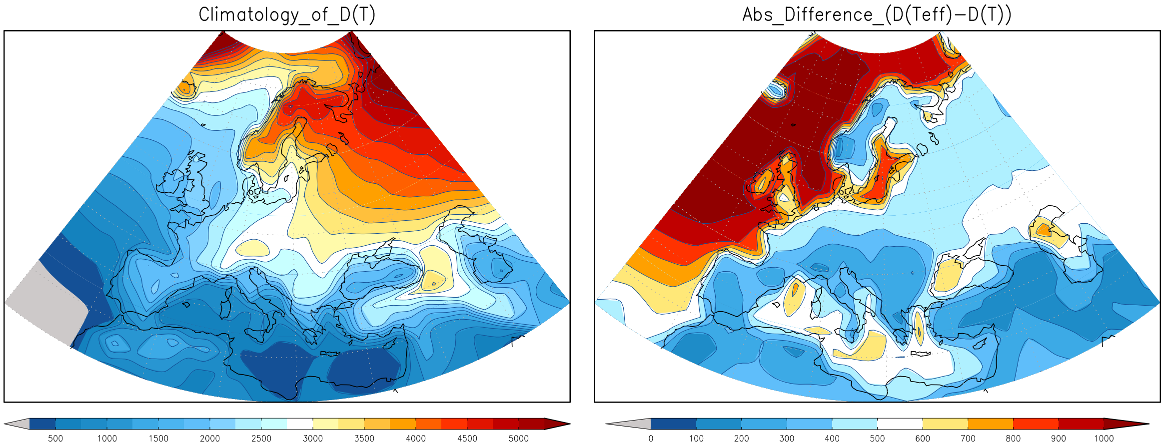

Figure 3.3: Heating degree days D. (left) Climatology of $D(\bar{T})$ (colors show total $D(\bar{T})$ for climatological winter half year). The threshold $T_{threshold} = 18.0$ was used to determine D [see (1.2)]. Data covers the entire ERA-40 data set. (right) Difference $D(T_{eff}) - D(\bar{T})$.

phy, the gradient in the area around the Netherlands is mainly East to West (warmer near the sea). The largest values of $D(\bar{T})$ are found over Greenland, Northern Europe and Siberia. Note that these areas also have the largest standard deviations (not shown).

2.2.1 Effect of the Wind It can be expected that the region Netherlands-France-British Isles is influenced significantly by the wind. This expectation is confirmed when we compare the climatology of $D(T_{eff})$ to the climatology of $D(\bar{T})$. The largest absolute differences (right panel in Figure 3.3) occur in the Northern Atlantic, the largest relative differences in the Mediterranean, (not shown). Our region, and generally all areas near the Atlantic coast show a strong increase. More inland the differences quickly become small, typically on the order of 1-10% of $D(\bar{T})$. Note that due to the definition of T_{eff}, $D(T_{eff})$ will always be larger than $D(\bar{T})$.

2.2.2 Anomalies In the previous section, we showed that the total number of heating degree days $D(\bar{T})$ computed for De Bilt shows large interannual variability (c.f. Wever, 2008). It is instructive to determine the spatial scale of anomalies $D' = D(\bar{T}) - D_{clim}(\bar{T})$ of the climatological mean $D_{clim}(\bar{T})$. To this aim we select the two years from the ERA-40 data set that produced the largest and smallest values of $D(\bar{T})$. The winters that were selected by this method are 1963 (largest $D(\bar{T})$) and 1990. Figure 3.4 contrasts these two extreme winters in terms of $D(\bar{T})$. Two features are directly apparent. First, the large spatial scale of the anomalies, both in case of the very cold, and the very mild winter. Second, the patterns observed for the two extreme winters look like the two ‘phases’ of a single pattern, with in case of the anomalously cold winter, a large positive anomaly in West and central Europe, and two accompanying negative anomalies at Greenland and the Turkish highland. The large scale in particular suggests that the atmospheric circulation probably plays an important role in determining the realized value of $D(\bar{T})$ for a single winter.

2.2.3 Pressure and Circulation patterns Figure 3.5 shows the large-scale low-level winter circulation anomalies accompanying the two anomalous winters. The anomaly is taken with respect to the multi-year winter-mean values shown in Fig. 1.1. Even though the time-average was taken over the entire winter half year (6 months), a large-scale signal appears in the cold-winter case, with the sea-level pressure anomlies ranging from nearly +9mbar at high latitudes and to -7mbar at low latitudes. The very mild winter of 1990 shows nearly the opposite anomaly field, with the pressures markedly lower than usual at high latitudes. Also shown are the snow-depth anomalies for the same winters. These show that only in case of the mild winter of 1990 there was significantly less snow than on average during the whole winter. The extremely cold winter of 1963 did not show such anomalous snow cover, the reason being that the Easterlies which accompanied the cold winter merely brought cold dry

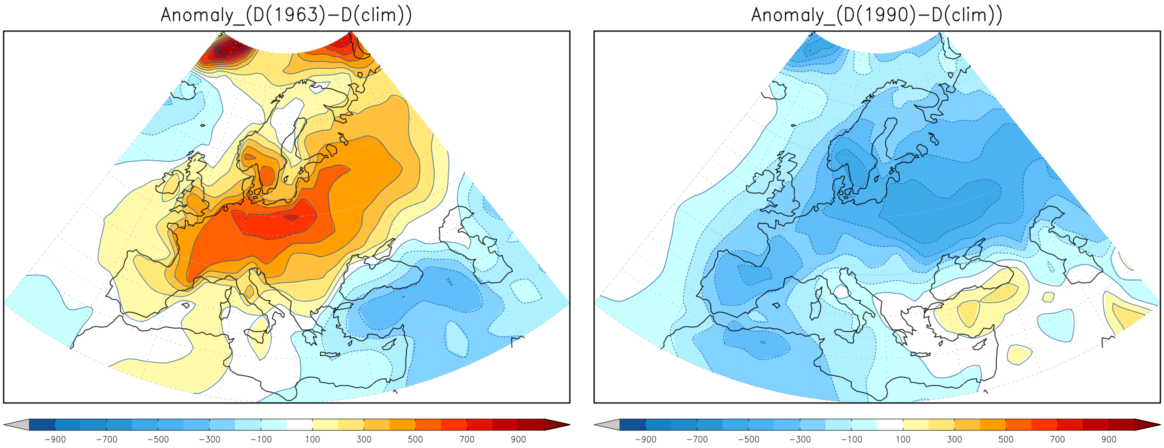

Figure 3.4: Heating degree days $D(\bar{T})$. Anomalies from climatology, $D - D_{clim}$. (left) The winter with largest $D(\bar{T})$ at De Bilt (1963). (right) The winter with smallest $D(\bar{T})$ at De Bilt (1990).

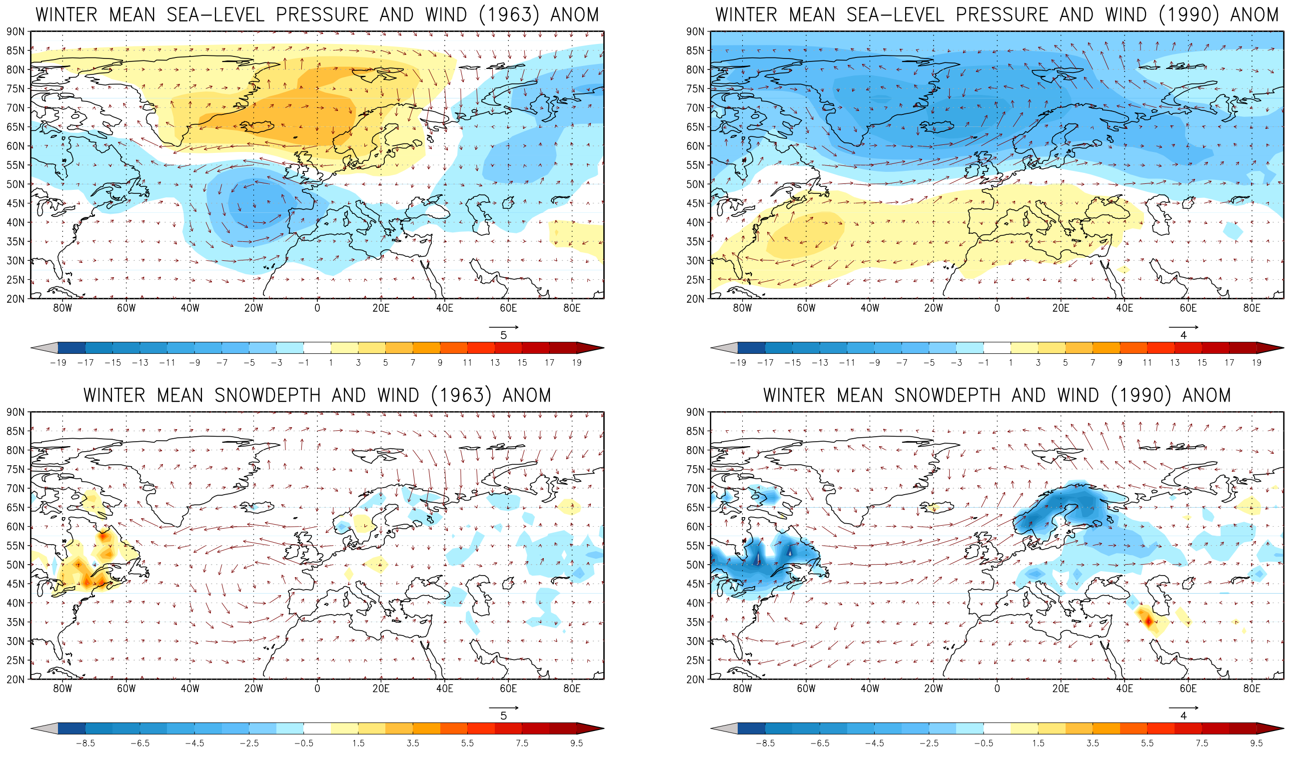

Figure 3.5: Mean sea-level pressure and 10M wind for the anomalous winters (October to March) of 1963 (left) and 1990 (right).

air.

3 Future projections

For the future perspective we use the ESSENCE data. It turns out that ESSENCE has a systematic bias compared to ERA-40. For $D(\bar{T})$ this is a warm bias, caused by the fact that the ocean has too large an influence on gridbox Netherlands in ESSENCE. For $D(T_{eff})$ ESSENCE has a much stronger cold bias. In this case the winds are too strong compared to ERA-40, leading to significantly larger values of $D(T_{eff})$. For this reason it was decided to correct for these systematic biases by adding an offset to the ESSENCE data such that the median of the 1951-2000 period of ESSENCE is equal to that of ERA-40.

3.1 Local scale

The left panel in figure 3.6 shows total winter $D(\bar{T})$ as a function of the years, which run from 1951 to 2100. The grey band describes the individual ensemble members, and the black line the ensemble mean. As with the ERA-40 results, the individual ensemble members exhibit large year-to-year fluctuations (autocorrelation functions drop rapidly to noise level). As we approach the end of the 21st century, one can notice a continuous decline in the winter $D(\bar{T})$ values, and this decline is nearly two times as strong as in the last period of the 20th century (-59 per decade and -29 per decade respectively). The ensemble spread is a measure for natural variability of the system. From this spread it is seen that approximately around 2050 the ensemble-mean line (black) falls outside the 'natural' variability (ensemble spread) of the period 1950-2000. By the end of the 21st century, even the coldest winters start to fall outside the natural variability range of $D(\bar{T})$ of the period 1950-2000.

The right panel in figure 3.6 shows $D(T_{eff})$. $D(T_{eff})$ also shows large year-to-year fluctuations and a decrease which is stronger near the end of 21st century than near the end of this century. The decrease per decade is similar to that of $D(\bar{T})$. This is a sign that most of the changes in $D(T_{eff})$ are cause by changes in daily-mean temperature and not by changes in windspeed. The signals obtained are robust to small changes in the geographical box over which the heating degree days have been computed.

Another way to represent the changes in D is in terms of the frequency distributions. They are shown in Fig. 3.7 for $D(\bar{T})$ and Fig. 3.8 for $D(T_{eff})$ (again the bias corrected data sets have been used). The ERA-40 distribution is shown in the red lines and the ensemble-mean for ESSENCE in black. The future projections show a shift of the entire distribution to lower values. Simultaneously, it appears that the distribution gets narrower (smaller standard deviation) and more negatively skewed. Further study of the distribution changes is considered out of skope of this study.

In summary, one can say that according to the ESSENCE data set, winters will become much milder near the end of the 21st century (Fig. 3.6). Having a look at the coldest winters near the end of the 21st century, one can see that these correspond roughly to the warmest winters of the second half of the 20th century. A formidable decrease (and a cause for worry for those who like ice-skating on nature ice). It has to be realized however, that the above results are obtained for a single model and assuming one particular emission scenario. Multi-model ensembles should be studied to assess the realism of the predicted change under the given future climate scenario.

3.2 Regional to Global scale

Figure 3.9 shows the differences between the ensemble mean climatology of $D(\bar{T})$ for the two periods 1950-2000 and 2051-2100 obtained with the ESSENCE data. Significant decreases of $D(\bar{T})$ are seen over most parts of European continent (Figure 3.9). The absolute decrease is largest at high latitudes. However, the relative decrease is largest over the Mediterranean region, which is mostly due to the fact that the threshold $T_{threshold}$ acts as a rigid cutoff. For large parts of the European continent the decrease is between 20 and 30 percent. It is worth mentioning that there are no gridpoints in the selected geographical region that show an increase in ensemble-mean value of $D(\bar{T})$. Zooming in on Western Europe, the predicted change roughly corresponds to a 2.5 ^{o}C increase of the daily mean winter temperature. To better appreciate the size of this change, one can say that winters which are exceptionally mild given current climate conditions (like the one showed in Fig. 3.4) will become "average" winters near the end of the 21st century.

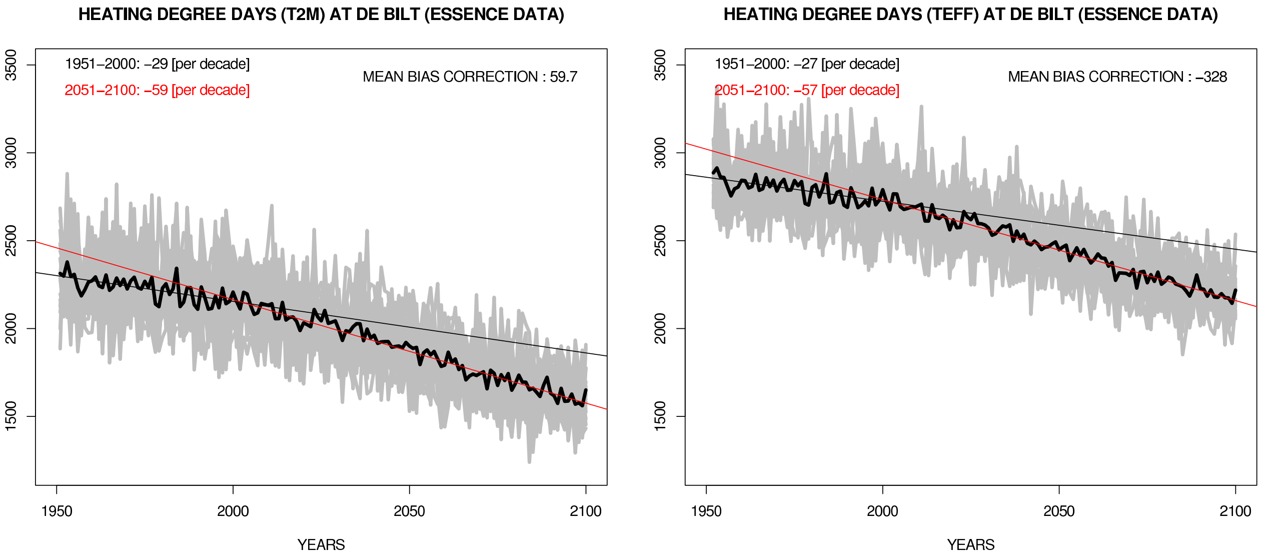

Figure 3.6: Total winter values of heating degree days $D(\bar{T})$ (left) and $D(T_{eff})$ (right) at gridbox Netherlands as a function in time according to ESSENCE data. The threshold $T_{threshold}$ = 18.0 was used to determine D [see (1.2)]. The grey lines show the individual ensemble members, the black line the ensemble mean. The thin lines show the least-square fit through the ensemble-mean data for the period 1951-2000 and the period 2051-2100.

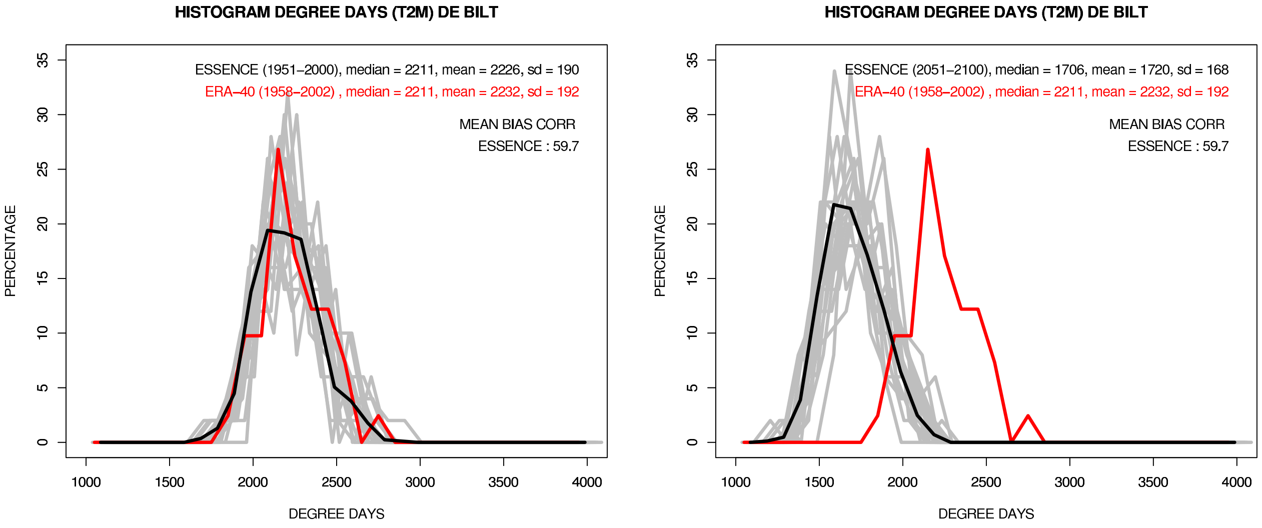

Figure 3.7: (left) Total winter values of heating degree days $D(\bar{T})$ at gridbox Netherlands as a function in time according to ESSENCE data. The threshold $T_{threshold}$ = 18.0 was used to determine $D(\bar{T})$ [see (1.2)]. The grey lines show the individual ensemble members, the black line the ensemble mean. The drawn line is the least-square fit through the ensemble-mean data for two periods (1951-2000 and 2051-2100).

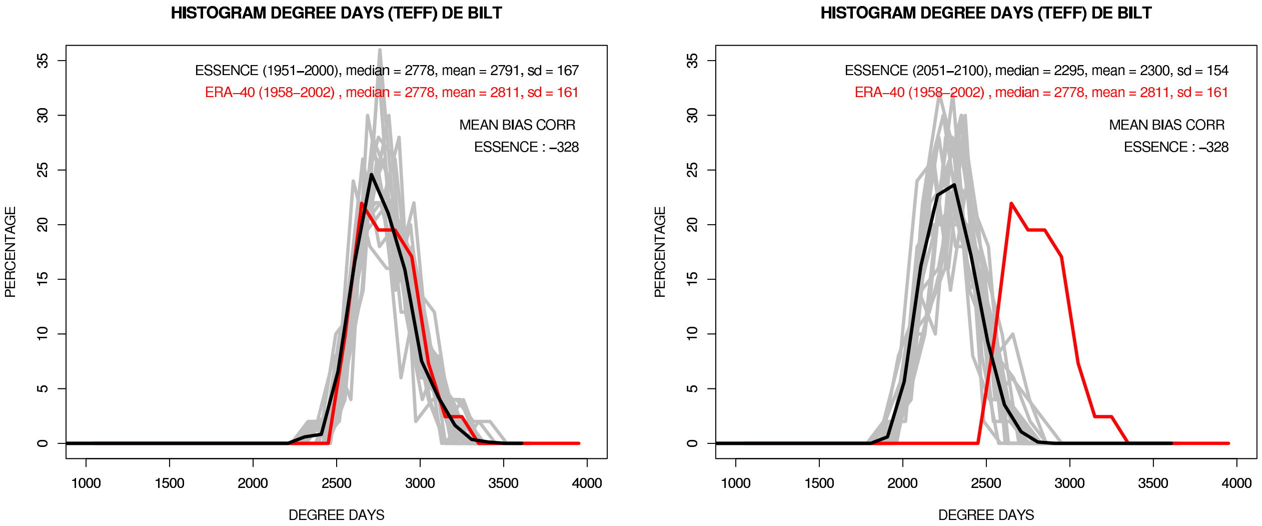

Figure 3.8: As in Fig. 3.7 but for $D(T_{eff})$.

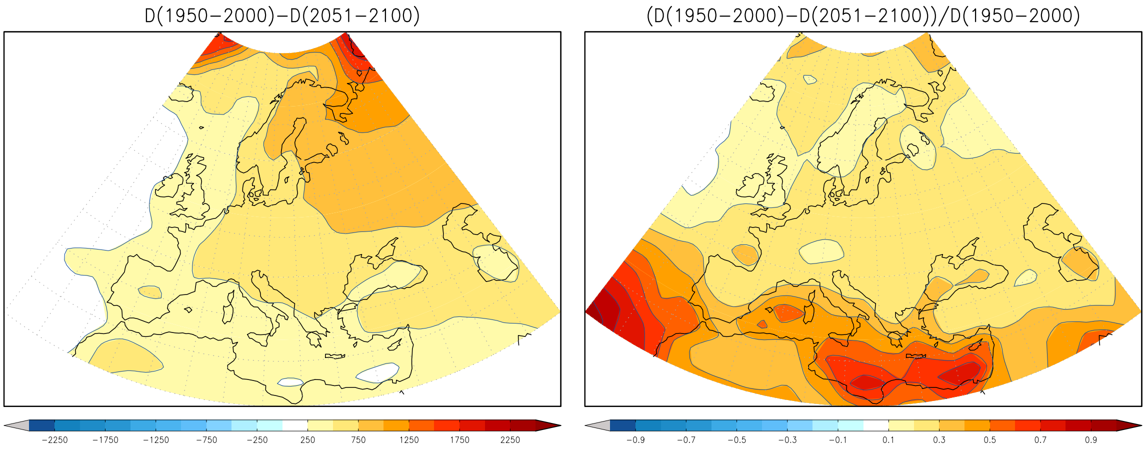

Figure 3.9: Absolute and relative differences between the ensemble-mean climatology of $D(\bar{T})$ for the periods 1950-2000 and 2051-2100, as obtained for the ESSENCE data and $T_{threshold}$ = 18 ^{o}C.

II

Cold Spells

4 Composite Analysis

Abstract. In this chapter the temperature and circulations associated with cold weather are analysed using composite analysis.

Conclusions. • The distribution of the 1% coldest days (measured by T_{eff}) has a clear bias towards the second half of the winter half year (4.1). • The climatological winter pressure pattern over the European region involves a large-scale low pressure system with its center near Greenland and Iceland, and high pressures near the Azores. This dipole produces the typical South-Westerly wind patterns in our region (Fig. 4.1). • The atmospheric state is said to be in a blocked condition, if the climatologically predominant Westerlies are absent or have reversed sign. • The composite of mean sea level pressure for anomalously cold days (coldest 1% T_{eff}) shows a markedly different pattern with high pressure over Scandinavia and Greenland, resulting in Easterly winds over the Netherlands (Fig. 4.1). This confirms the hypothesis that extreme cold days most often occur during atmospheric blocking. • The composite pattern is robust to changes in the geographical location where the threshold criterion is applied (Fig. 4.5). Similar results are also obtained if the coldest daily mean temperature would have been taken. • The evolution of the composite shows that the blocking high pressure pattern exists for at least two weeks at virtually the same geographical location (center between Iceland and Scandinavia), before being advected away over Europe. This period is long enough to set very cold air on transport that has its origin in Siberia (Fig. 4.3). On the western flank of the high pressure pattern, Greenland experiences anomalous heating.

1 Introduction

In a composite analysis, particular threshold criteria are applied in order to select only particular, often extreme events. The rationale is simple: if there is a systematic tendency of for example cold days at De Bilt to coincide with easterly winds over the Netherlands, than this will show up in the mean field of all events meeting the selection criterion (the composite field). The expectation is that non-systematic, random configurations are filtered by taking the mean over a large-enough sample. Therefore, a composite analysis can reveal whether a particular phenomenon (such as for instance anomalously low temperatures in De Bilt) appears also as an anomaly in other meteorological fields such as wind field or pressure. For obvious reasons the composite comprises of only one single pattern. However, by having a look at the standard deviation, one can get an estimate of how robust this pattern is for the events that meet the criteria.

In this study we focus on the atmospheric state that accompanies anomalously cold days over the Netherlands. Cold days are measured here in terms of anomalously low T_{eff} (lowest 1%). The question is whether characteristic large-scale pressure and temperature patterns appear, and how they evolve. In particular we are interested in the relation between cold days and the phenomenon of atmospheric blocking.

2 Present day

We only use those days that belong to the 1% coldest days (measured in terms of T_{eff}). For the ERA-40 dataset this produces a threshold $T_{eff} < -7.4$ ^oC, and one gets a composite over 165 days. Table 4.1 shows how these days are distributed over the different months of the year. January is generally the coldest month, with more than 50% of the days contributing to the composite record. There is a clear bias of the cold days to occur in the second half of the winter half year. The bias is caused primarily by the proximity of the Netherlands to the North Sea and the Atlantic Ocean, and the fact that it takes a long time too cool down large sea areas.

The next step is to compute composite patterns for other fields. The fields that were chosen are mean sea level pressure (mslp) and 2-meter temperature (t2m). Mslp is chosen because of its relation to the circulation, and t2m is chosen to emphasize the geographical relation between cold air over the Netherlands, and cold air elsewhere. Since most of the days for the 1% coldest days occur in January, it is instructive to discuss the January climatology of mslp and t2m first (left panel in Figure 4.1). The most distinct feature of the mslp-field (contours) is the low-pressure cell which reaches its minimum between Iceland and Greenland (termed the Icelandic low). The South-Westerly flow associ-

Coldest (T_{eff})	Oct	Nov	Dec	Jan	Feb	Mar	Apr
1 % coldest	0%	0.6%	20.6%	51.5%	26.1%	1.2%	0%
5% coldest	0%	4.8%	22.7%	32.4%	30.0%	9.8%	0.2%

Table 4.1: Monthly distribution of 1% and 5% coldest days ($T_{eff} < -7.4$ ^{o}C and $T_{eff} < -2.7$ ^{o}C respectively) at De Bilt, according to the ERA-40 data.

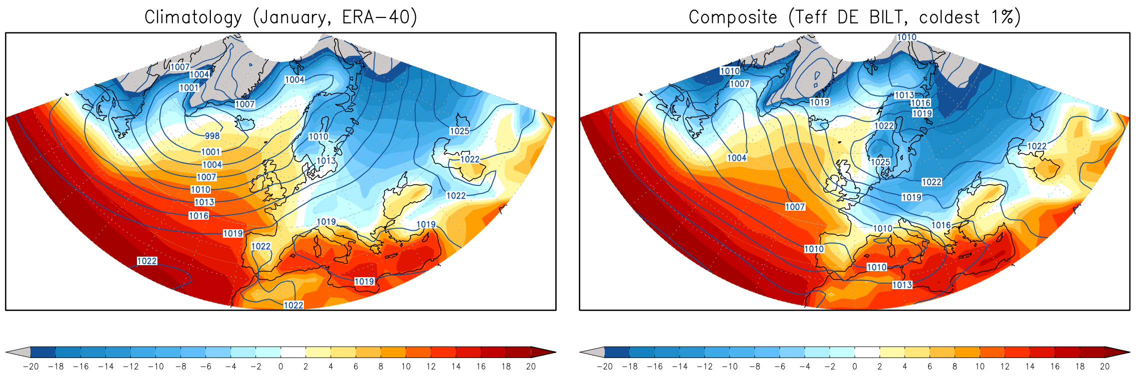

Figure 4.1: (left) January climatology of mean sea-level pressure (contours, interval 3 mbar) and 2-meter temperature in ^{o}C (colors). (right) composites of mean sea level pressure (contours, interval 3 mbar) and 2m temperature in ^{o}C.

ated with this low-pressure brings relatively warm and moist air to Western Europe. Further in land the mean January temperatures quickly drop below zero ^{o}C. Also visible is the Azores High, a region of high pressure in the Atlantic off the coast of Morocco.

The right panel of Figure 4.1 shows the composite patterns for mslp (contours) and 2m temperature (colors) that accompany the coldest 1% days at De Bilt. Both the mslp and t2m pattern are markedly different from the January climatology. Clear features of the pressure field are (1) the high-pressure cell above Scandinavia exceeding 1025 hPa, and (2) the complete change of structure of the Icelandic Low. Its pressure minimum has moved South Westwardly. More importantly, rather than being almost zonally oriented, the pressure contours now move Southward and return over the Mediterranean.

The differences between climatology and the extremes can be analyzed in more detail by looking at their difference. Figure 4.2 shows the composites for the anomaly fields. The anomalies have been taken with respect to the multiyear monthly mean fields. The most striking feature of the mslp anomaly field is the presence of the large-amplitude dipole, with a positive maximum between Scandinavia and Iceland, and a minimum over Spain. With this mslp pattern, the temperature anomalies are hardly surprising: negative over Western and central Europe and positive over Greenland. Also visible is the positive anomaly over Turkey, caused by the South-Westerly flow bringing in air that originated over Africa.

2.1 *Pattern evolution*

In this section we examine the time-evolution of the composite fields. By this we mean that for each record that satisfies the composite criterion (coldest 1% T_{eff}), we extract the 10 days prior to this event, as well as the 10 days after the event. As a further restriction we do not allow the events to overlap. In the algorithm we first select the coldest day on record, and subtract the 10 days prior and after from the record. Then we seek the next coldest day (that still satisfies the 1% coldest T_{eff} condition) and repeat the process. Using the procedure leaves us with a total of 48 21-day events, approximately once every winter.

Figure 4.3 shows the evolution for a few selected times. More than a week prior to the event anomalously high pressure above Iceland is clearly visible together with a cold-air reservoir over the continent. In the following days, Easterly windspeeds increase and the high pressure cell gains amplitude. Simultaneously the negative pressure anomaly over the Mediterranean increases in amplitude, further enhancing the

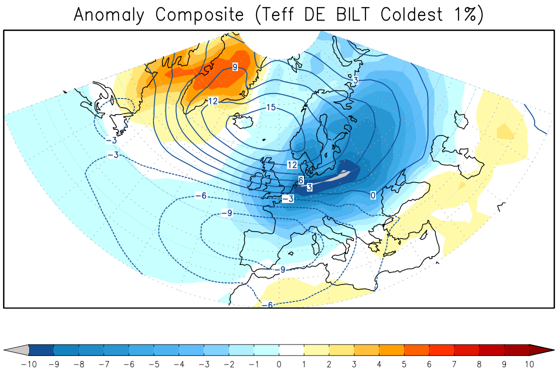

Figure 4.2: Composites of mean sea level pressure (contours, interval 3 mbar) and 2m temperature in ^{o}C for the anomalies from monthly-mean climatology.

Easterly winds. As the cold air anomaly from Northern Siberia moves in a south-westerly direction, its amplitude increases (remember that air of the same cold temperature will correspond to a larger anomaly in the Netherlands than e.g. in Poland). At the day of the extreme event (the right panel on the second row), negative temperature anomalies of more than 10^{o}C are observed. In our area the isobars are close together, implying that there is significant wind. After the event, the decay is a relatively rapid process. The high pressure anomaly moves eastward and decays in a couple of days. Note that because of the constraint of the events being isolated, the panel at $t = T$ differs slightly from that shown in Figure 4.2. The differnce that has most effect is the location of the pressure maximum, and the associated temperature anomalies.

2.2 *Sensitivity tests*

2.2.1 Different percentiles In this section we briefly look at what changes if we study the composite of the 5% coldest quantile, rather than the 1% coldest days of the previous section. Now the threshold is $T_{eff} < -2.7$ ^{o}C and many more days are included (see Table 4.1. January and February stand out from the other winter months and there is a stronger bias of the cold days to occur in the second half of the winter half year: none of the 5% coldest days occurs in October, whereas nearly 10 percent in March (and even some in April). The composites for mean sea-level pressure and 2-meter temperature are shown in Figure 4.4 and are similar indeed to those shown for the 1% coldest days. The positive maximum of the mslp anomaly pattern however is much weaker and also displaced eastwardly in the direction of Scandinavia.

2.2.2 Geographical location To test the sensitivity of the composite fields to the location of the extreme (De Bilt), we compute the composite record for a larger domain that includes parts of Germany and Northern France (latitudes 47.5-55, longitudes 5-10). The composite fields are shown in Figure 4.5. From the similarity of the patterns in this figure to those in Figure 4.2 one can conclude that the patterns are not very sensitive to the location of the extreme. Note however that substantially different patterns would result if one would select a completely different geographical area such as for instance Spain, or the Balkan.

3 Future projections

In this section we report on the future projections of the coldest days obtained using ESSENCE data. We now focus on the 1% coldest days of daily mean $\bar{T}$. Table 4.2 shows how these days are distributed over the different months of the year. Two things are immediately apparent: First, there is a significant difference between ERA-40 and ESSENCE, with the ESSENCE having a stronger bias towards the second half of the winter half year than ERA-40. Second, the future projections made with ESSENCE show no significant changes for the future. It is not uncommon for climate models to have problems simulating details at locations where there are strong contrasts, for instance between land surface and sea surface. Netherlands are situated at such a transition. Apparently in the climate model used to produce ESSENCE, Netherlands experiences

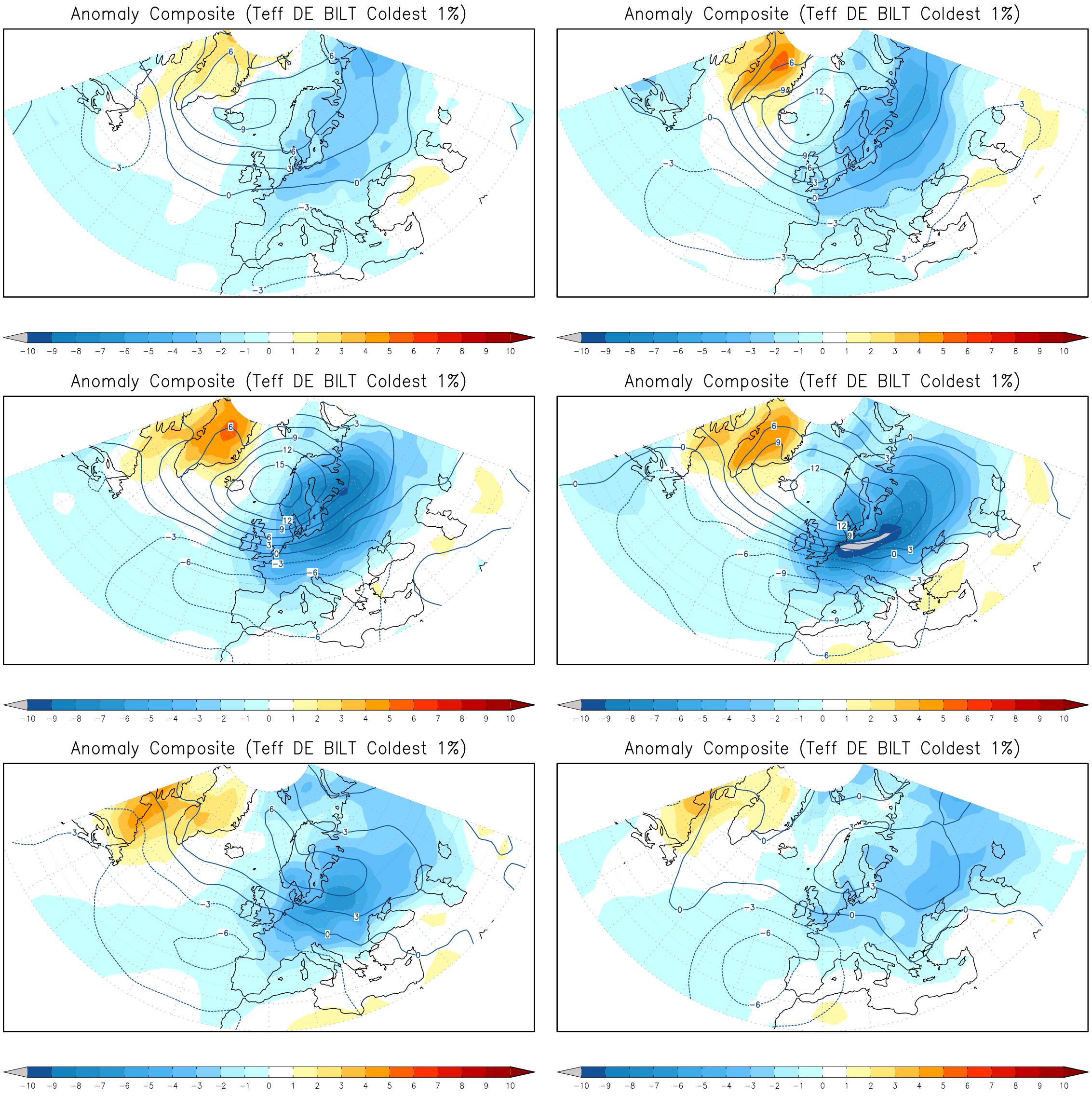

Anomaly Composite (Teff DE BILT Coldest 1%)

Anomaly Composite (Teff DE BILT Coldest 1%)

Anomaly Composite (Teff DE BILT Coldest 1%)

Anomaly Composite (Teff DE BILT Coldest 1%)

Anomaly Composite (Teff DE BILT Coldest 1%)

Anomaly Composite (Teff DE BILT Coldest 1%)

Figure 4.3: Time evolution (T-9,T-5,T-2,T,T+2,T+5) of the composites of mean sea level pressure (contours, interval 3 mbar) and 2m temperature in ^{o}C for the anomalies from monthly-mean climatology.

Coldest ($\bar{T}$)	Oct	Nov	Dec	Jan	Feb	Mar
ERA-40	0%	0%	20.2%	52.4%	23.8%	3.6%
ESS-NOW	0%	0.5%	13.0%	42.1%	38.4%	6.1%
ESS-FUT	0%	0.5%	12.9%	41.9%	38.3%	6.4%

Table 4.2: Distribution of 1% coldest days ($\bar{T}$) at De Bilt, according to ERA-40 and ESSENCE DATA (ESS-NOW=1951-2000 and ESS-FUT=2051-2100).

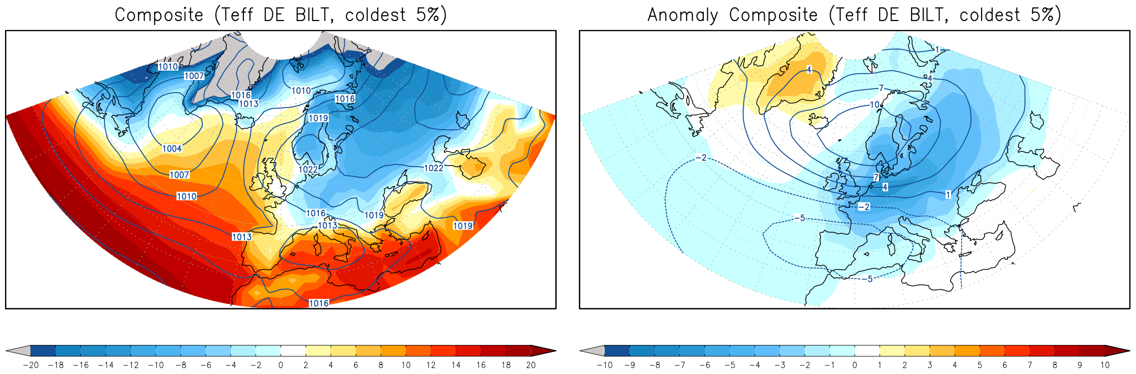
Composite (Teff DE BILT, coldest 5%)

Anomaly Composite (Teff DE BILT, coldest 5%)

Figure 4.4: Composites of mean sea level pressure and 2m temperature (left) full fields; (right) anomalies from monthly-mean climatology.

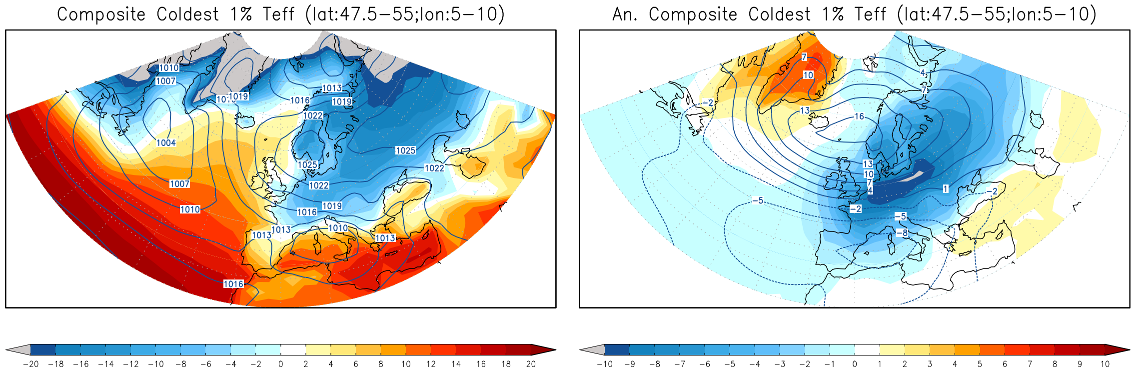
Composite Coldest 1% Teff (lat:47.5−55;lon:5−10)

An. Composite Coldest 1% Teff (lat:47.5−55;lon:5−10)

Figure 4.5: Composites of mean sea level pressure and 2m temperature (left) full fields; (right) anomalies from monthly-mean climatology. The composites were obtained for the 1% coldest days for the region bounded by latitudes 47.5-55 and longitudes 5-10.

too much influence from sea, with the obvious consequence (sea cools only slowly in time) that the coldest days will occur later in the season. Of course it could also be the case that the ERA-40 period experienced incidentally many early cold days, but the former argument is more likely to be the case. Indeed, by selecting the coldest days of the gridbox directly to the east of Netherlands, most of the difference between ERA-40 and ESSENCE in the 'timing' of the coldest days disappears.

5 Cluster analysis

Abstract. In this chapter we use a statistical tool called cluster analysis, to further examine the mean sea level pressure composite associated with anomalously cold days in De Bilt.

Conclusions. • Cluster analysis of the mslp fields that are associated with the 1% coldest days reveals two distinct patterns (Fig. 5.2). • The first pattern (dubbed G) has its high pressure over Greenland and forms a tripolar structure with accompanying lows to the south-west and north-east of the high. The second pattern (S) has a much larger horizontal scale with the center high pressure region located over Scandinavia and Russia, and low pressures over Greenland. • Both clusters G and S are related to conditions where the prevailing climatological westerly winds over the Netherlands and a large part of central Europe are blocked. Moreover, each of these is immediately recognised as being relevant to winter time coldspells by a well trained meteorologist.

1 Introduction

Composite analysis, as explained in chapter 4, is a basic tool for getting information about the mean meteorological state of events that match threshold criteria (e.g., cold days). If the variance of the composite pattern is relatively large, this could indicate that there are more (physically) distinct patterns satisfying the same threshold conditions. However, composite analysis is not able to distinguish between those patterns. In this chapter we use cluster analysis to disentangle them.

1.1 Cluster analysis Method

Cluster analysis is a statistical technique in which patterns are grouped according to some similarity measure. Many clustering algorithms exist. In this chapter we use Ward's hierarchical clustering algorithm (Ward, 1963), which has been applied to atmospheric data for instance in Cheng and Wallace (1993). The main steps are outlined below.

One starts with all patterns of the time series. Each of these patterns consists of M grid points and can therefore be represented as a single array of M values $\mathbf{a}^k = (a_1^k, \cdots, a_M^k)$. In order to determine which patterns have to be clustered, a similarity measure is computed. In case of Ward's method, the similarity between two patterns $\mathbf{a}^k$ and $\mathbf{a}^l$ is defined as the Euclidean difference between the patterns

$$d^2(\mathbf{a}^k, \mathbf{a}^l) = ||\mathbf{a}^k - \mathbf{a}^l||^2 = \sum_{j=1}^{M} (a_j^k - a_j^l)^2, \qquad (1.1)$$

such that a small value of $d^2(\mathbf{a}^k, \mathbf{a}^l)$ means a high similarity*. Advantages of taking the Euclidean distance as a measure of the similarity between patterns are its simplicity and objectivity. A possible drawback is that $d^2(\mathbf{a}^k, \mathbf{a}^l)$ is not necessarily physically the most relevant measure of pattern similarity.

Initially all patterns are assigned their own cluster, which is denoted by A^k. In each step of the clustering algorithm, two existing clusters are merged. To determine which clusters are to be merged, the heterogeneity within each cluster is analysed. This 'within-cluster heterogeneity' is computed with respect to its centroid, the mean of all maps that form cluster $A^k = (\mathbf{a}^{k_1}, \cdots, \mathbf{a}^{k_n})$:

$$\bar{\mathbf{a}}^k = \frac{1}{n} \sum_{r=1}^{n} \mathbf{a}^{k_r}. \qquad (1.2)$$

Heterogeneity within cluster A^k is defined as the squared Euclidean distance from the cluster centroid

$$E_k = \sum_r d^2(\bar{\mathbf{a}}^k, \mathbf{a}^{k_r}), \qquad (1.3)$$

where the summation is over all patterns that form the k-th cluster. Therefore, $E_k = 0$ before any clustering has occurred. At each step in the analysis, the next two clusters to be merged will be those that yield minimum increase in $E = \sum_k E_k$. The clustering is finished if after $N - 1$ clusterings all patterns are clustered in one big cluster, whose centroid is given by the composite mean field, and where E is the total variance summed over all grid points and times. Further details can be found

---

*Another simple measure of similarity would be to take the inner-product $\mathbf{a}^k \cdot \mathbf{a}^l$.

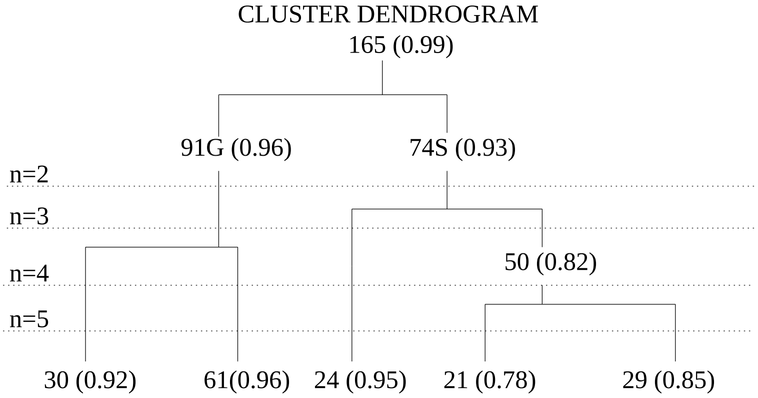

Figure 5.1: Dendrogram or 'family-tree' for Ward clustering of the 1% coldest days in De Bilt, obtained from ERA-40 data. The number shows the number of days spent in each of the clusters (For each level of clustering, the total number of days equals 165). The number in between brackets denotes the value of the reproducibility parameter, as explained in Section 1.1. The intersections of the dashed lines with the vertical lines denote the clusters at a particular value of n, whose patterns are shown at the n-th row in Fig. 5.2 (from left to right). The clusters labelled as G and S are further discussed in the main text.

in Cheng and Wallace (1993).

Cluster Reproducibility As always when using statistical techniques, it is important to investigate the robustness of the results. To this aim Cheng and Wallace (1993) determine a reproducibility parameter for each cluster. This parameter basically measures the degree to which the clusters can be reproduced by randomly selected subsamples of the data. More specifically, the reproducibility parameter is determined from the following steps. 1) Randomly select 50 % of the data. 2) Compute clusters for this randomly selected subset of the data. 3) For all cluster centroids i that appeared in the final stages of the clustering process[*] of the original dataset, compute the correlation coeffcients R_{ij} between centroid i and those (j) obtained with the randomly selected subset of the data. 4) For each cluster i of the original data set, the maximum $max_j(R_{ij})$ (i is fixed) is a measure of the reproducibility of that cluster. 5) Repeat steps 1 to 4 for n times[†]. For each cluster, the mean value of the n correlation coefficients thus obtained, is called the reproducibility parameter of that pattern (Cheng and Wallace, 1993).

2 Present day

As in the chapter 4 on composite analysis, we select those days that belong to the 1% coldest days (measured in terms of T_{eff}). For the ERA-40 dataset this produces a threshold $T_{eff} < -7.4$ ^{o}C, and a composite that includes 165 daily mean pressure patterns. The cluster dendrogram or 'family-tree' is shown in Fig. 5.1. It gives a concise summary of the last four merges and the reproducibility of the clusters. The cold-days mslp climatology (i.e., the composite-mean pattern) as well as some of the clusters are shown in Fig. 5.2. The second row of panels shows that the composite mean pattern falls apart in two main clusters that are markedly different. The first cluster (labelled G) shown at $n = 2$ is characterized by a tripolar structure, with high surface pressures over Greenland and a very marked low pressure system over the North Atlantic and the polar Ocean. The second cluster (labelled S) has a dipole structure, with high pressure over Scandinavia and Siberia and low pressure over a large part of Greenland and the Atlantic. Both clusters have a very high reproducibility and meteorologists would recognise the above two types as being associated with (potentially) very cold days in winter times. Note that in both cases, the winds over the Netherlands have an Easterly component. Comparing the monthly distribution of the G and S cluster (Table 5.1) shows that both clusters occur predominantly in January. The G pattern appears to occur more frequently later in the season than the S pattern. However, at this stage it is difficult to say something about the statistical significance of this difference.

---

[*] We used the patterns that appeared in the last 4 merges.

[†] We used $n = 250$.

Coldest (T_{eff})	Oct	Nov	Dec	Jan	Feb	Mar
ERA-40	0%	0.6%	20.6%	51.5%	26.6%	1.2%
G	0%	0%	18.8%	50.5%	28.7%	2.0%
S	0%	1.6%	23.4%	53.1%	21.9%	0.0%

Table 5.1: Monthly distribution of 1% coldest days (T_{eff}) at De Bilt when partitioned in to the two clusters G and S (see main text for explanation). Source: ERA-40 data set.

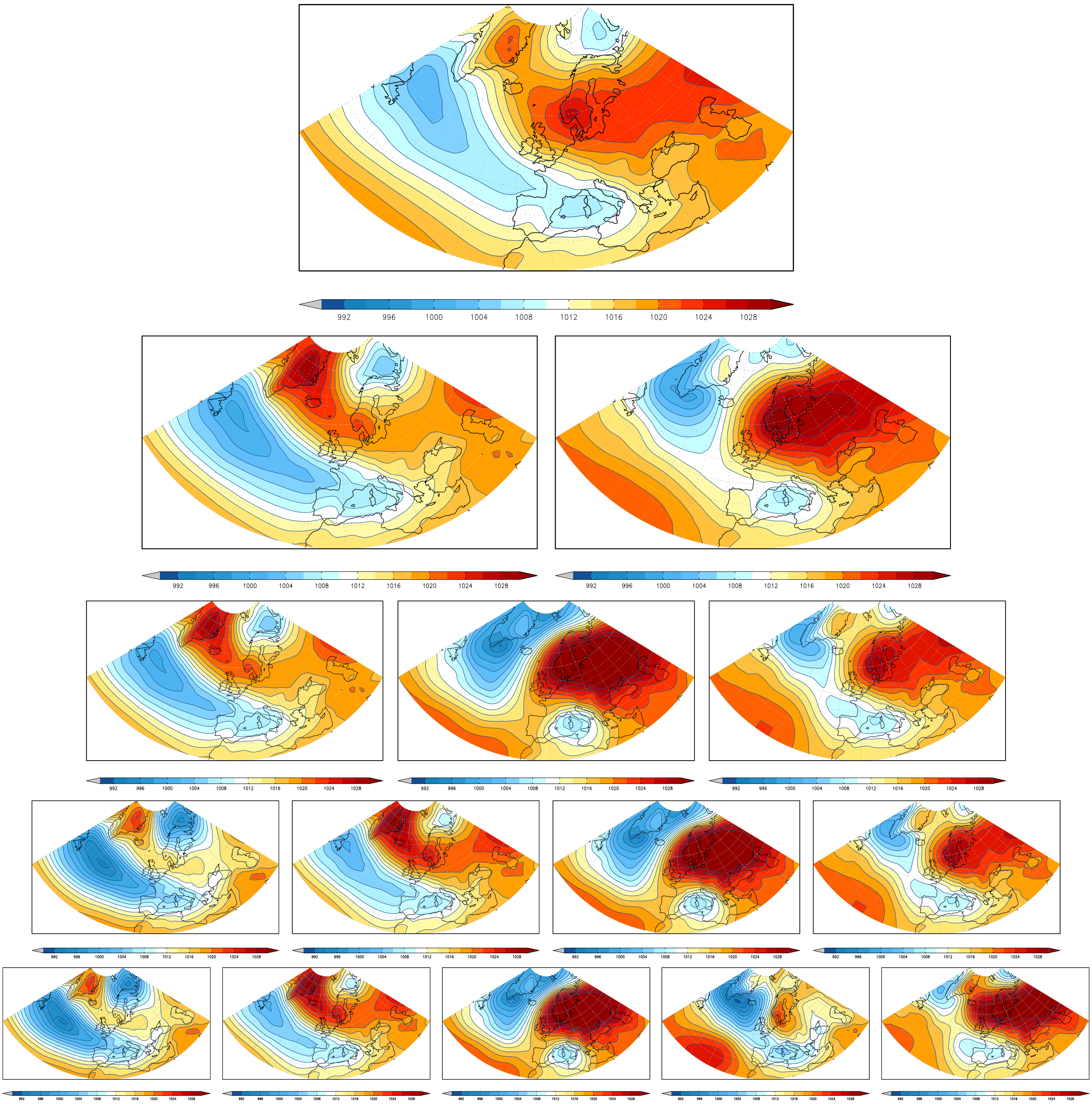

Figure 5.2: Composites of mean sea level pressure (in mbar) for the coldest 1% days T_{eff} at de Bilt and the clusters that formed at the last stages of the clustering process. The cluster tree is shown in Fig. 5.1. Top to bottom: climatological mean ($n = 1$); $n = 2$; $n = 3$; $n = 4$; $n = 5$. Contours show mslp (high pressures are red).

Both patterns are found at the earlier stages of the clustering process. At $n = 3$, one can see that the S pattern forms from a merge between one cluster with a very large amplitude mslp dipole, and one with a smaller amplitude center directly above Scandinavia. At $n = 4$ the G pattern is formed from two patterns, where in the first the low pressures over the Atlantic and polar Ocean are very high, and in the second the Greenland high is dominant and basically has extensions over Scandinavia towards Russia. At $n = 5$ one can notice the first appearance of a pattern (number 4 from the left) in which the high pressure anomaly has a smaller spatial scale, with only a weak high pressure system centered above Scandinavia. However for these latter patterns the reproducibility drops below 0.80. These are not discussed.

3 Future projections

In this section we discuss the mean sea-level pressure (mslp) climatology and dominant clusters obtained for the coldest days at De Bilt (now measured with $\bar{T}$). Two data sets have been used: ERA-40 (1958-2002) and ESSENCE (1951-2000 period and 2051-2100 period). For each of these we have computed its particular 1% threshold temperature. The mslp climatology of the coldest days is shown in Fig. 5.3. First observe that the mslp climatologies for all three data sets are very similar indeed. This is surprising if one takes into account that the mean winter temperatures in the future projections are several degrees higher than those for current climate conditions. The difference between ERA-40 and ESSENCE (Fig. 5.4) shows a more or less systematic (i.e., period independent) bias of ESSENCE towards slightly higher pressures above the Arctic Ocean and Mediteranean and lower pressures near Iceland and South-East Europe. The difference between the future and present-day ESSENCE data (right panel Fig. 5.4) does not show signs of any significant trends.

The dominant clusters obtained for ESSENCE and ERA-40 are shown in Fig. 5.5, which confirm that under the projected change, in future the dominant types of weather associated with cold days, can still be classified in terms of a G (Greenland) pattern, and an S (Scandinavia-Russia) pattern. From this one can conclude that according to ESSENCE blocking will likely play an equally important role in the future as it plays in present day climate. The main difference will be that the future blocked states advect air to our regions that is less cold than it is in current climate.

Remark The results obtained in the previous section (obviously) would have been different if one would have chosen to take an absolute threshold value instead of the percentage. In that case, it would have been found that only a very few cases in the future period would meet the threshold criterium. It is most likely that to get very cold temperatures in future (e.g. similar to the 1% threshold values of present day) one requires a stronger blocked state.

Remark We have already discussed the difference in monthly distribution of the coldest days in Table 4.2 (p34), where it was noted that ESSENCE produces relatively more cold days in February than ERA-40. The reason that the ESSENCE 2-meter temperature distribution for the Netherlands is biased compared to ERA-40, is related to the overestimation of the influence of the nearby sea and ocean. This bias also plays a role here, leading to differences in the monthly distribution of the G and S clusters (Table 5.2). ESSENCE apparently fails to produce enough S patterns in January, but over-estimates both pattern types in February and March. Most of this difference in 'timing' can be corrected for by taking temperature data from ESSENCE for a gridbox slightly more in land.

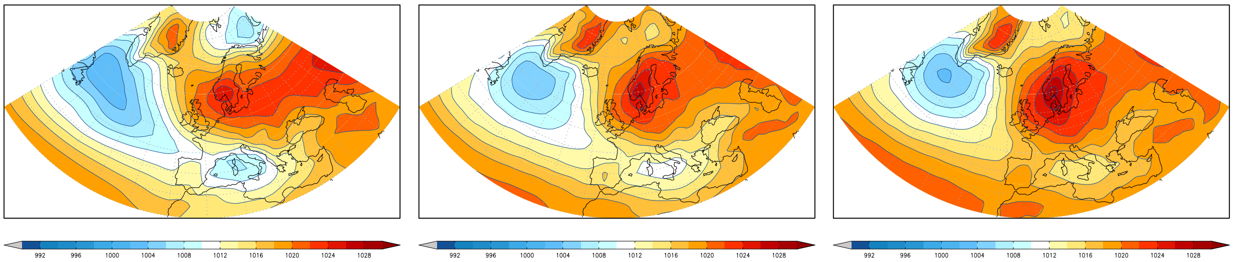

Figure 5.3: Mean sea level pressure climatology (in mbar) for the 1% coldest days (measured by $\bar{T}$) at de Bilt. (left) ERA-40 (middle) the 1951-2000 period of ESSENCE (right) the 2051-2100 period of ESSENCE. Note that each dataset has been computed with its own 1% threshold.

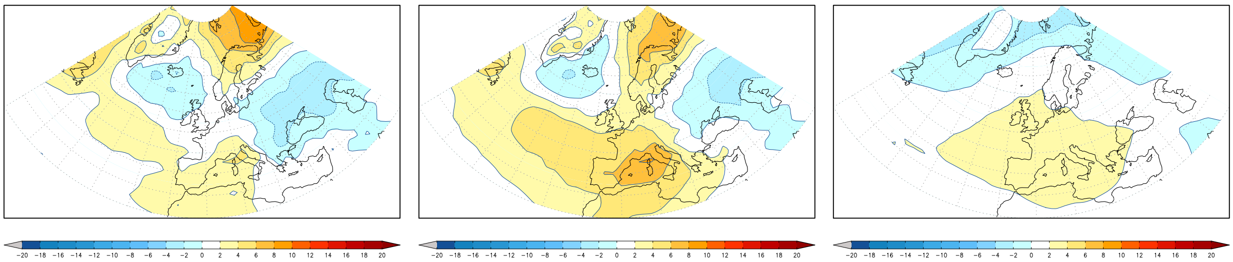

Figure 5.4: (left) difference between the 1951-2000 period of ESSENCE and ERA-40 (middle) difference between the 2051-2100 period of ESSENCE and ERA-40. (right) difference ESSENCE(2051-2100)-ESSENCE(1951-2000).

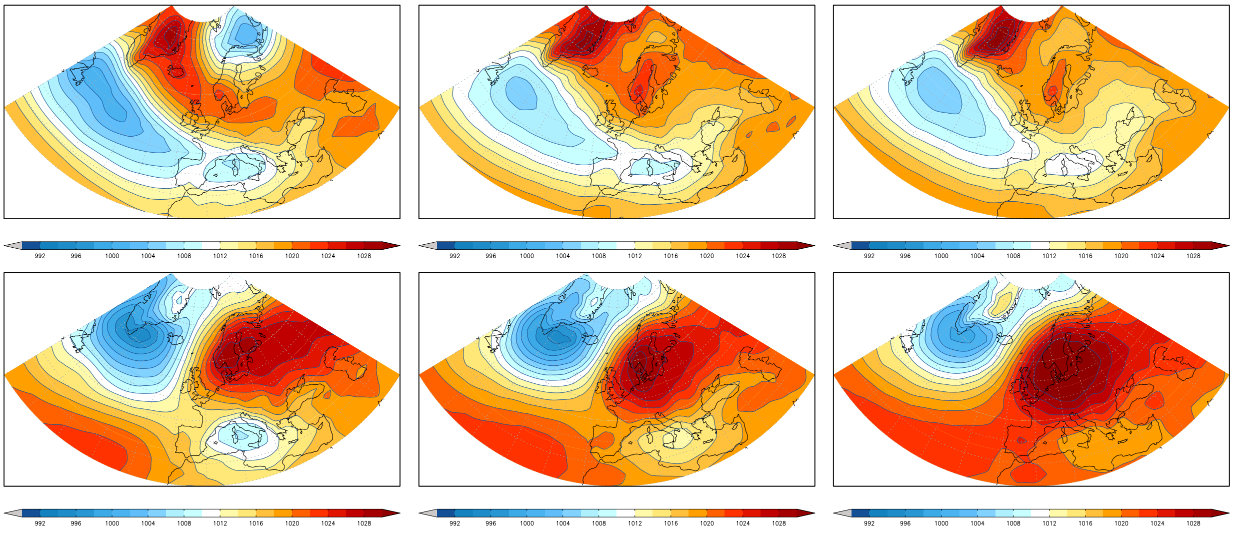

Figure 5.5: Dominant clusters of mean sea level pressure (in mbar) for the coldest 1% days (measured with $\bar{T}$) at de Bilt. (left) ERA40 (middle) 1951-2000 period of ESSENCE (right) 2051-2100 period of ESSENCE. Top: G cluster; bottom: S cluster. The G and S cluster are explained in the main text.

Coldest ($\bar{T}$)	Oct	Nov	Dec	Jan	Feb	Mar
ERA-40	0%	0%	20.2%	52.4%	23.8%	3.6%
G	0%	0%	22.5%	43.7%	29.6%	4.2%
S	0%	0%	18.6%	58.8%	19.6%	3.1%
ESS-NOW	0%	0.5%	13.0%	42.1%	38.3%	6.1%
G	0%	0.5%	12.9%	41.8%	38.3%	6.4%
S	0%	0.5%	13.2%	42.5%	38.2%	5.6%
ESS-FUT	0%	0.5%	12.9%	41.9%	38.3%	6.4%
G	0%	0.4%	11.8%	43.7%	37.1%	7.1%
S	0%	0.7%	14.2%	39.9%	39.7%	5.6%

Table 5.2: Monthly distribution of 1% coldest days ($\bar{T}$) at De Bilt when partitioned in to the two clusters G and S (see main text for explanation). Source: ERA-40 data set.

6 Persistence

Abstract. In this chapter we look at the persistence of cold weather.

Conclusions. • The probability p for a cold spell (defined here as belonging to the 5% coldest days) to last another day increases with the duration of the event (Fig. 6.1-6.2). In other words, it is more likely to stay cold if it is already cold for some days. The optimum ($p \sim 0.8$) is found for events that last already between 10 and 20 days. The probability that it will stay cold for n more days, given that it is already cold for some days, quickly decreases with increasing n. • Return periods were also estimated for cold spells of a given duration (Fig. 6.3). It is found that the return period for cold spells of ten days is about 5 years, and that of a cold spell of twenty days about twenty years. • Under the A1B scenario and using climate model output (ESSENCE data), there is a significant drop in the probability for a cold-spell event to last another day for the period 2051-2100 (Fig.6.4), if the same threshold is chosen as used for the reference period (1958-2002 obtained using ERA40 data). • Some of the above-mentioned drop in probability can be accounted for by using the 2051-2100 period's own 5% temperature threshold (which is almost 4 degrees higher). If that threshold is used for the future scenario, it is still observed that the probability for getting a prolonged cold period becomes smaller (Fig. 6.5). For events that last only a few days, the changes in p are not observed.

1 Introduction

Often a cold day is followed by another. That this is the case can in fact be easily understood if one looks at the amplitude and spatial scale of the composite mslp and t2m patterns (see the image at frontpage): It will take at least a couple of days to decay a positive mslp anomaly of almost 20 mbar. During that time, winds will have easterly components, which transport cold air from the continent to our region.

A simple measure for the probability of getting another cold day can be obtained by computing event durations for events meeting certain threshold criteria. The number of n-day series will be denoted by $\#(n)$. The probability for an n-day event to last at least m days longer (denoted as $P_m(n)$) is then given by the ratio of $\#(n+m)$ and $\#(m)$:

$$P_m(n) = \frac{\#(n+m)}{\#(m)} \tag{1.1}$$

To get a not too small record, we select the 5% coldest days (measured with T_{eff} or with $\bar{T}$), which for the ERA-40 data set consists of 820 days.

2 Present day

Figure 6.1 shows $P_m(n)$ as computed with (1.1), obtained for De Bilt and various values of m. The black line shows $P_1(n)$, or the probability of an n-day event to last at least one day longer. There is a broad plateau of high probabilities, $P_1(n) > 0.8$ for values of n between 12 and 29, with the absolute maximum for $n = 18$. If we increase m (the number of days the cold period has to last longer) to values around a week ($m = 7$), probabilities (obviously) decrease rapidly: For $m > 7$ (the chance to last at least one week longer) the probability $P_m(n) < 0.5$ for all values of n. The plateau becomes a peak with a maximum between 12 to 14 days.

Remark One has to be careful interpreting Figure 6.1 as will be explained now. The middle panel in Figure 6.1 shows a partitioning of the 5% coldest days at De Bilt into single, continuous events of a particular length, obtained from the daily mean data, without furter time filtering. The right panel shows the number of n-day series that can be formed using the data and which is used to compute $P_m(n)$ (Note the logarithmic scale). Of the total of 259 individual events listed in the middle panel, more than 40% lasted only a single day. There is a sharp decrease in the number of longer-lasting events, with only very few events (in fact 3) lasting longer than 15 days. Therefore, the entire asymptotic statistics shown in Figure 6.1 is based on studying only one exceptionally long event (34 days). The data-set simply consists of too few long-lasting events for the results at large n to be significant.

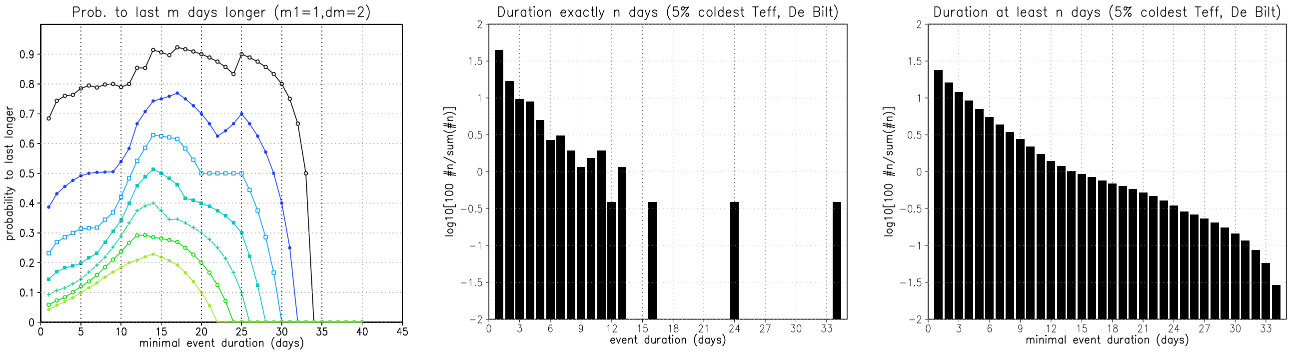

Figure 6.1: (left) Probability $P_m(n)$ of getting at least m more cold days (5% coldest T_{eff} at De Bilt) if at least n days of cold days (on the x-ordinate) have occurred prior. The different curves show $P_m(n)$ for various m: black-green correspond to $m = 1, 3, \cdots 13$. (middle) Percentage of events that last exactly n days (notice the log10 scale, 1=10%,0=1%,-1=0.1%). (right) Percentage of n-day series that can be formed.

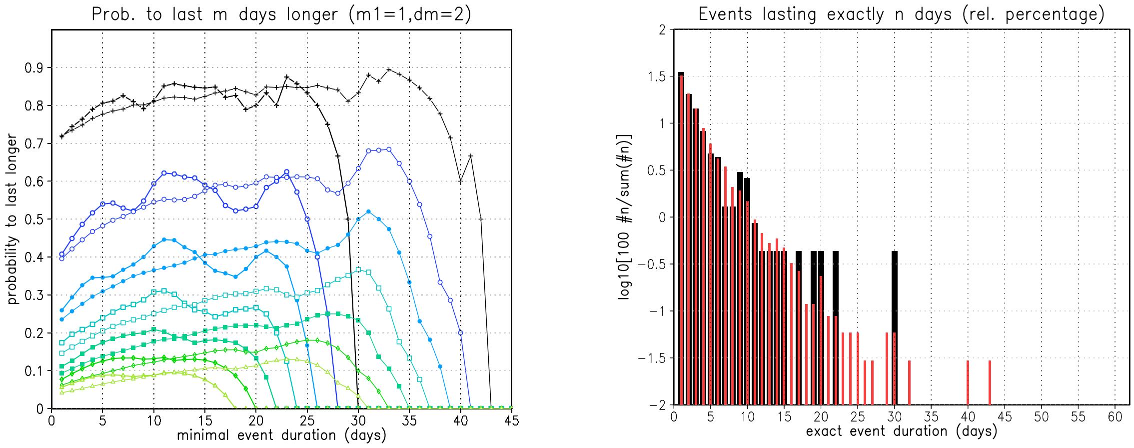

Figure 6.2: Same as Fig. 6.1 but for a threshold value (-0.12^{o}C) based on the 5% coldest t2m from ERA-40. (left) ERA-40 data (thick) and ESSENCE 1950-2000 data (thin). (right) Relative percentage of events that last exactly n days. black: ERA-40. red: ESSENCE.

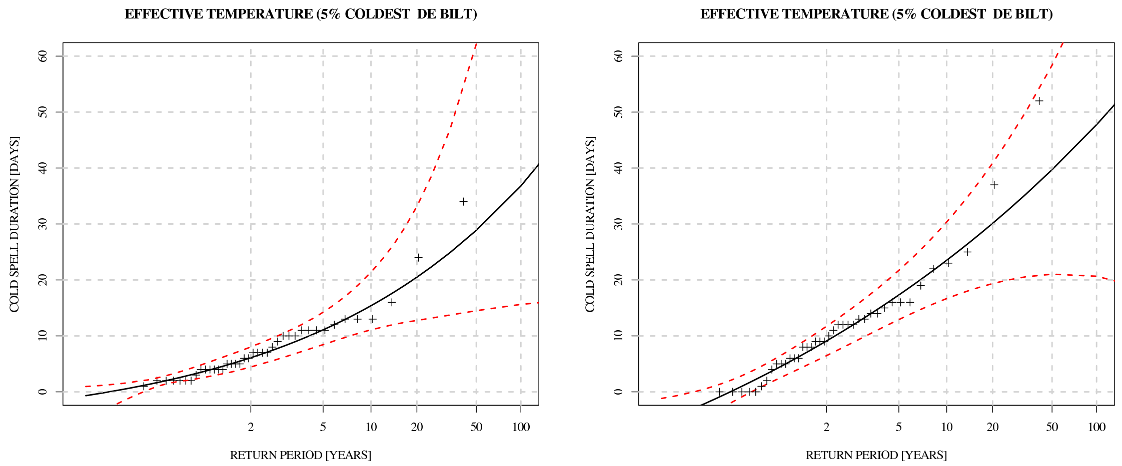

Figure 6.3: (left) Return periods for cold spells in De Bilt (defined as events in which effective temperature reaches the lowest 5% level). Data source: ERA-40 1960-1999 period. Marks denote data, full line denotes the fitted gev-distribution. The dashed lines show a 95% confidence interval determined by the bootstrap method. (right) Same but first applying a 7-day running mean filter through the data.

Remark The ERA-40 results were compared to those obtained with the ESSENCE dataset (Sterl et al., 2008). Since ESSENCE consists of many more years than ERA-40, we expect the ESSENCE dataset to potentially better sample the distribution of longer (and very rare) events. Results are shown for t2m in Figure 6.2, where we used the same threshold value for each dataset, namely that obtained from the ERA-40 dataset (-0.12^{o}C). Comparing ERA-40 to ESSENCE, one can conclude from the left panel in Figure 6.2 that the probabilities for cold events to last at least one to three days longer (black and dark blue lines) agree reasonably well for shortlasting events (the tail is not present in ERA-40), but that ERA-40 overestimates (or ESSENCE underestimates) the chances that short cold periods will continue for at least 5 days more. The curves obtained for the ESSENCE data set are clearly smoother, resulting from the much longer record. The right panel in Figure 6.2 shows the relative percentage of events lasting exactly n days, from which the left panel results have been constructed. This picture confirms that ERA-40 and ESSENCE have approximately equal (relative) amount of shortlasting cold events, but that ERA-40 has relatively more long-lasting events. Because of the short observational record of ERA-40, it remains difficult to judge whether ERA-40 or ESSENCE is closer to the true distribution.

2.1 *Return periods*

Return periods for cold-spells (effective temperature within lowest 5% levels) were investigated, by computing for each winter season the longest (continuous) cold-spell event. A generalized extreme value (gev) distribution was fitted through the data (see e.g., Wever (2008)) and 95% confidence intervals were estimated with a bootstrapping method. Results are shown in the form of a Gumbel plot in Figure 6.3. On the basis of this figure it is found that the return period for cold spells of ten days is about 5 years, and that of a cold spell of twenty days about twenty years. The same plot compiled from t2m data, is very similar to that obtained for T_{eff}. Note that the longer the duration of the event, the wider the confidence limits spread apart. Longer time series are required to more properly sample the distribution at longer return periods. The above discussion does not state anything about the chance of having more than one cold spell within one winter. Often, cold winters are characterized by not one but several cold spells, with some intermediate warmer weather. One way to include this aspect is to apply a running-mean time filter of several days (e.g. 7) before fitting the gev-distribution. This has been done in the right panel of Fig.6.3. This figure shows longer cold spells for a given return period, thereby confirming that in some winters cold spells are sometimes intercepted (the longest cold spell in the right panel occurred in the winter of 1963, the longest cold

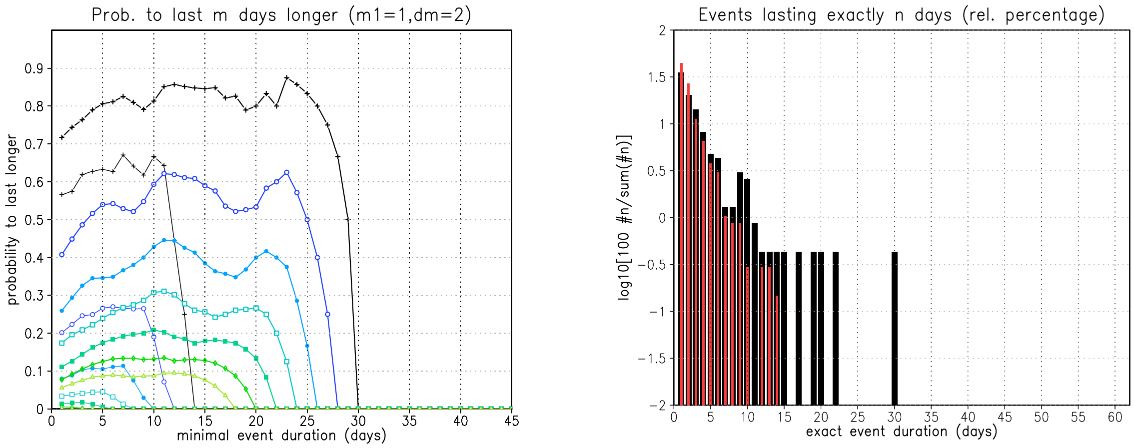

Figure 6.4: Same as Fig. 6.2 but for a threshold value (-0.12^{o}C) based on the 5% coldest t2m from ERA-40. (left) ERA-40 (thick) and ESSENCE 2051-2100 period (thin). (right) Relative percentage of events that last exactly *n* days. black: ERA-40. red: ESSENCE.

spell in the left panel in the winter 1997).

3 Future projections

The probabilities for getting another cold day are computed for the 2051-2100 period of the ESSENCE data set. The same absolute value of the threshold obtained from ERA-40 (-0.12^{o}C) is used, to emphasize how big the changes are compared to the reference climate. The results are shown in Figure 6.4. As one can see, for the chosen threshold there is a rather dramatic decrease in the number of longlasting cold periods, implying that also the probability for events to last longer greatly decreases.

Western Europe is heating significantly under the A1B scenario. It makes sense to investigate the probabilities where the percentiles are created for each dataset individually. For instance, if there are significant differences between the 1950-2000 and 2051-2100 period of ESSENCE, this could hint to changes in weather regimes for those periods. The left panel in Figure 6.5 shows the probability plot for cold periods to last longer if one uses for each data set its own 5% threshold. For the 1950-2000 period of ESSENCE, the 5% percentile at De Bilt is 0.63^{o}C, nearly 0.7^{o}C above that of ERA-40. For the 2051-2100 period it is 4.3^{o}C. The most important difference between present-day and future projections are related to the very long-lived cold periods that last longer than a month. The future dataset contains less of these events. In this sense it appears that the weather in the future climate may be getting more variable. For small values on the x-axis (events that last up to five days), however, the differences are small and probably not statistically significant.

To see whether similar changes occur on the other side of the distribution, namely at the warmest end of the t2m record at De Bilt, the right panel in Figure 6.5 shows the same result but obtained for the 5% warmest days at De Bilt. From this figure one can notice that there seem to be less changes in on the warm side of the distribution. It will be a subject of further research to investigate whether changes in blocking persistence are mainly found in winter times.

Remark In the discussion of the ESSENCE data, a single temperature threshold was used based on the 5% coldest days of all ensemble members together. An alternative choice would be to use different thresholds for the different ensemble members. Experimenting with different temperature thresholds (not shown) reveals that particularly the results for events with a duration longer than 20 days are quite sensitive to the choice of threshold. This is another indication that more research is needed to investigate the significance of the differences between the present-day and future ESSENCE period, as shown in Figure 6.5.

Remark It should be stressed that all previous results have been obtained with a single climate model and for a specific emission scenario (A1B). Further research and in particular multi-model experiments should be

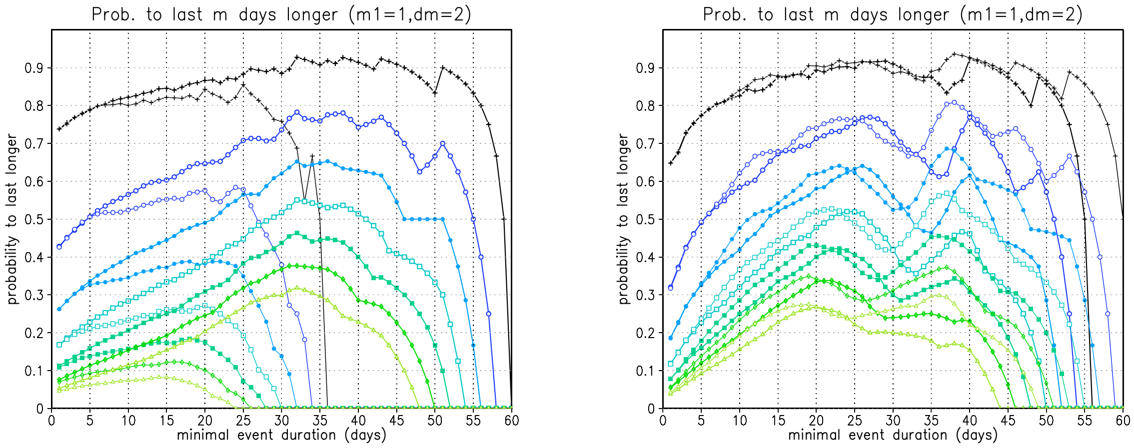

Figure 6.5: As in Figure 6.4 but with the 5% coldest (left) and 5% warmest (right) thresholds determined for each data set separately. thick: ESSENCE 1950-2000. thin lines: ESSENCE 2051-2100.

conducted to (in)validate the above results.

Remark An estimation of the return periods of cold spells of given duration should still be performed for the ESSENCE data.

B Bibliography

Cheng, X. and J. M. Wallace, 1993: Cluster analysis of the Northern hemisphere wintertime 500-hPa height field: Spatial patterns. *J. Atmos. Sci.*, **50**, 2674–2696.

Hurk, B., A. M. G. Klein Tank, G. Lenderink, and et al., 2006: KNMI Climate Change Scenarios 2006 for the Netherlands. Tech. rep., Koninklijk Nederlands Meteorologisch Instituut (KNMI).

Klein Tank, A. M. G. and G. Lenderink, 2009: Klimaatverandering in Nederland; Aanvullingen op de KNMI '06 scenario's. Tech. rep., KNMI, De Bilt.

Lorenz, E. N., 1963: Deterministic nonperiodic flow. *J. Atmos. Sci.*, **20**, 130–141.

Sterl, A., C. Severijns, and H. Dijkstra et al., 2008: When can we expect extremely high surface temperatures? *Geophys. Res. Lett.*, **35 (L14703)**, doi:10.1029/2008GL034071.

Uppala, S. M., P. W. Kallberg, and A. J. Simmons et al., 2005: The ERA-40 Re-analysis. *Quart. J. Roy. Meteorol. Soc.*, **131**, 2961–2013.

Ward, J., 1963: Hierarchical grouping to optimize an objective function. *J. Amer. Statist. Assoc.*, **58**, 236–244.

Wever, N., 2008: Effectieve temperatuur en graaddagen: Klimatologie en klimaatscenario's. KNMI publicatie 219.

A complete list of all KNMI-publications (1854 – present) can be found on our website

www.knmi.nl/knmi-library/knmipub_en.html

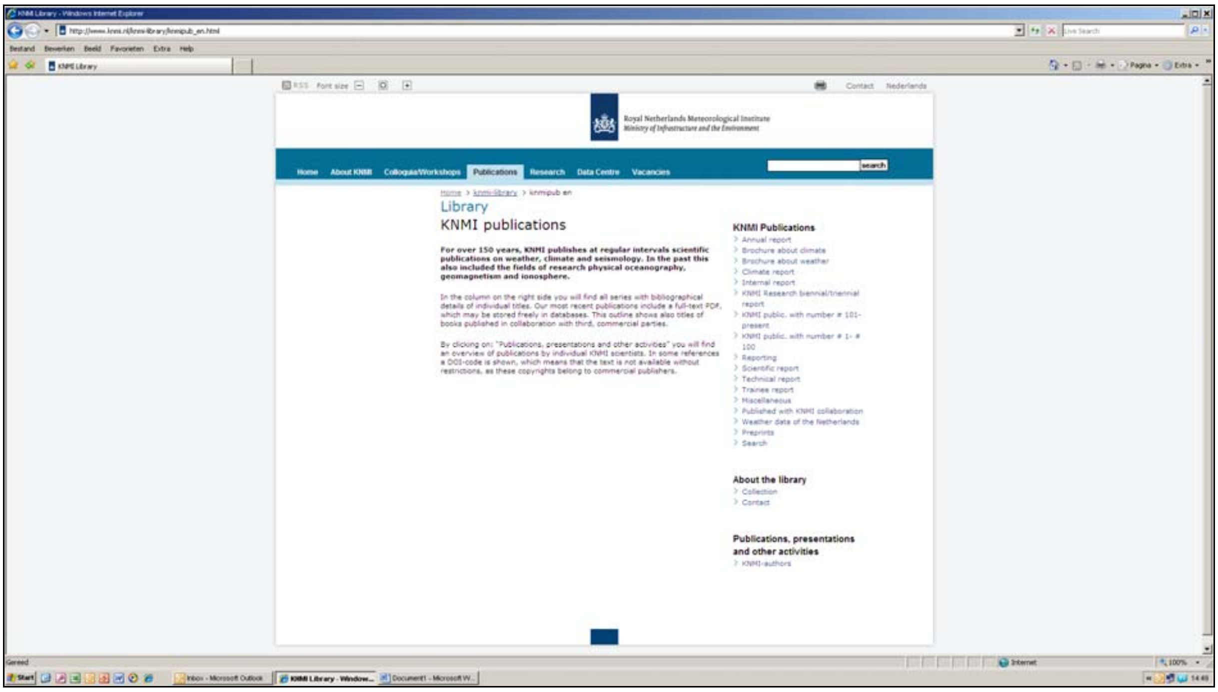

For over 150 years, KNMI publishes at regular intervals scientific publications on weather, climate and seismology. In the past this also included the fields of research physical oceanography, geomagnetism and ionosphere.

In the column on the right side you will find all series with bibliographical details of individual titles. Our most recent publications include a full-text PDF, which may be stored freely in databases. This outline shows also titles of books published in collaboration with third, commercial parties.

By clicking on: "Publications, presentations and other activities" you will find an overview of publications by individual KNMI scientists. In some references a DOI-code is shown, which means that the text is not available without restrictions, as these copyrights belong to commercial publishers.

The most recent reports are available as a PDF on this site.